The Pennsylvania State University
The Graduate School
College of Engineering

# DESIGN OF INTERPLANETARY TRAJECTORIES WITH MULTIPLE SYNERGETIC GRAVITATIONAL ASSIST MANEUVERS VIA PARTICLE SWARM OPTIMIZATION

A Thesis in
Aerospace Engineering
by
Matthew J. Shaw



Submitted in Partial Fulfillment
of the Requirements
for the Degree of

Master of Science

August 2018

The thesis of Matthew J. Shaw was reviewed and approved* by the following:

Robert G. Melton
Professor of Aerospace Engineering
Thesis Advisor

David B. Spencer
Professor of Aerospace Engineering

Amy R. Pritchett
Professor of Aerospace Engineering
Head of the Department of Aerospace Engineering

*Signatures are on file in the Graduate School.

# Abstract

The design capacity for synergetic gravity assists (powered flyby's) changes the type of possible optimal trajectories to distant planets. Heuristic optimization methods have potential to produce useful trajectories for design purposes. The application of Particle Swarm Optimization (PSO) is used to determine optimal mission trajectories from Earth to planets of interest, subject to synergetic gravity assist maneuver(s) in between. In order to verify the results from PSO, past missions are re-examined from a new design perspective. The trajectories designed by aid of PSO are compared to the trajectories involving the real mission dates. Test results are obtained for Voyager 1, Voyager 2, and Cassini. The results closely resemble those of actual mission data, providing support for the new design method involving PSO and synergetic gravitational assists. The computation of these solutions offers the unique benefit of costing one to two minutes of wall clock time with standard desktop or laptop computing systems. In addition to the past missions that are considered for re-design, the work then extends the design method to a newly proposed multiple gravity-assist mission from Earth to Saturn that could take place within the next few years. Two different mission timelines are considered. Direct routes and multiple gravity assist (MGA) routes to Saturn are compared. The best solutions from PSO for the MGA routes are on an order of one half to one third the propellant cost as compared to the direct routes for the launch and arrival dates chosen. Finally, consideration for promising future research directions involving PSO and synergetic gravity assist maneuvers is discussed.

# Table of Contents

# List of Figures

# List of Tables

# List of Symbols

| | |
|---|---|
| $a$ | Semi-major axis of orbit, two-body problem. |
| $a^-,\ a^+$ | Semi-major axis into flyby planet, out of flyby planet, synergetic flyby. |
| $a_{AVG}$ | Average semi-major axis. |
| $\Upsilon$ | Direction for the first point of Aries. |
| $\beta$ | Angle between asymptote and LOA for hyperbolic orbit, two-body problem. |
| $\beta^-,\ \beta^+$ | Angle between asymptote and LOA into flyby planet, out of flyby planet, synergetic flyby. |
| $\mathbf{b}_{lower}$ | Array of lower bounds in PSO algorithm for possible flyby Julian dates for a MGA mission. |
| $\mathbf{b}_{upper}$ | Array of upper bounds in PSO algorithm for possible flyby Julian dates for a MGA mission. |
| $c_C$ | Cognitive acceleration coefficient for the PSO algorithm. |
| $c_I$ | Inertia acceleration coefficient for the PSO algorithm. |
| $c_S$ | Social acceleration coefficient for the PSO algorithm. |
| $C$ | Center of geometric diagrams, two-body problem. |
| $\mathbf{C}_1\ (\epsilon)$ | Direction cosine matrix to transform from ICRF to SICF. |
| $\mathbf{C}_3\ (\delta)$ | Direction cosine matrix for rotating velocity vector into hyperbolic orbit through turn angle to the velocity vector out of the hyperbolic orbit. |

| | |
|---|---|
| $CD$ | Calendar date. |
| $\delta$ | Turn angle of hyperbolic orbit determined from geometry, two-body problem. |
| $\delta^*$ | Turn angle determined from a dot product operation on the velocity vectors into and out of a synergetic flyby. |
| $\Delta$ | Impact parameter, aiming radius, two-body problem. |
| $\Delta^-,\ \Delta^+$ | Impact parameter or aiming radius into flyby planet, out of flyby planet, synergetic flyby. |
| $\Delta_A$ | Absolute tolerance, Newton-Raphson schemes. |
| $d$ | Day of Calendar date. |
| DCM | Direction cosine matrix. |
| $\epsilon$ | Obliquity of the ecliptic. |
| $\epsilon^-,\ \epsilon^+$ | Specific energy into flyby planet, out of flyby planet, synergetic flyby. |
| $e$ | Eccentricity of orbit, two-body problem. |
| $e^-,\ e^+$ | Eccentricity into flyby planet, out of flyby planet, synergetic flyby. |
| $E$ | Eccentric anomaly of orbit, two-body problem. |
| $E_0$ | Initial guess of eccentric anomaly, Newton-Raphson scheme. |
| $E_i$ | Eccentric anomaly of current iteration, Newton-Raphson scheme. |
| $E_{i+1}$ | Eccentric anomaly of next iteration, Newton-Raphson scheme. |
| $f(E_i)$ | Elliptical orbit function to be driven to zero, Newton-Raphson scheme. |
| $f'(E_i)$ | Derivative of the elliptical orbit function to be driven to zero, Newton-Raphson scheme. |
| $f_1$ | First vector function component to be driven to zero for a multivariate Newton-Raphson scheme. |

| | |
|---|---|
| $f_2$ | Second vector function component to be driven to zero for a multivariate Newton-Raphson scheme. |
| $F$ | Occupied focus, two-body problem. |
| $\mathbf{F}$ | Vector function of unknown variables to be driven to zero for a multivariate Newton-Raphson scheme. |
| $F'$ | Vacant focus, two-body problem. |
| $f, \dot{f}, g, \dot{g}$ | The Lagrange coefficients. |
| GA | Gravitational assist, gravitational assist manuever. |
| $h$ | Magnitude of specific angular momentum, two-body problem. |
| $\vec{h}_{\oplus}$ | Specific angular momentum vector of Earth's orbit with respect to the Sun. |
| $\vec{h}_{sc/\otimes}$ | Specific angular momentum vector with respect to the planet. |
| $h_p$ | Altitude of periapse at flyby encounter of a planet. |
| $h_{p,min}$ | Minimum acceptable altitude of periapse at flyby encounter of a planet. |
| $hr$ | Hours of Calendar date. |
| $H$ | Hyperbolic anomaly of orbit, two-body problem. |
| $H_0$ | Initial guess of hyperbolic anomaly, Newton-Raphson scheme. |
| $H_i$ | Hyperbolic anomaly of current iteration, Newton-Raphson scheme. |
| $H_{i+1}$ | Hyperbolic anomaly of next iteration, Newton-Raphson scheme. |
| $f(H_i)$ | Hyperbolic orbit function to be driven to zero, Newton-Raphson scheme. |
| $f'(H_i)$ | Derivative of the hyperbolic orbit function to be driven to zero, Newton-Raphson scheme. |
| $i$ | Orbital inclination with respect to an inertial coordinate frame. |
| ICRF | International Celestial Reference Frame. |

| | |
|---|---|
| $J$ | Cost function for the PSO algorithm. |
| $\mathbf{J}$ | Jacobian for a system of unknown variables in a multivariate Newton-Raphson scheme. |
| $J_{Best,G}$ | Global best cost function for entire swarm within PSO algorithm. |
| $J_{Best,j}$ | Personal best cost function for an individual particle within PSO algorithm. |
| $J_j$ | Cost function for an individual particle within PSO algorithm. |
| $JD$ | Julian date. |
| $JD_A$ | Julian date of arrival for a MGA mission. |
| $JD_{FB_1}$ | Julian date of flyby encounter 1 (GA 1) for a MGA mission. |
| $JD_{FB_2}$ | Julian date of flyby encounter 2 (GA 2) for a MGA mission. |
| $JD_{FB_{N-1}}$ | Julian date of flyby encounter $N-1$ (GA $N-1$) for a MGA mission. |
| $JD_{FB_N}$ | Julian date of flyby encounter $N$ (GA $N$) for a MGA mission. |
| $JD_L$ | Julian date of launch for a MGA mission. |
| LOA | Line of apsides. |
| $\mu$ | Gravitational parameter of central body, two-body problem. |
| $min$ | Minutes of Calendar date. |
| $mo$ | Month of Calendar date. |
| $M$ | Mean anomaly of orbit, two-body problem. |
| MGA | Multiple gravitational assists, multiple gravitational assist manuevers. |
| $n$ | Mean motion of orbit, two-body problem. |
| $N_{iterations}$ | Number of iterations in the PSO algorithm. |
| $N_{FB}$ | Number of flyby encounters (GAs) to solve for a MGA mission. |
| $N_{LP}$ | Number of Lambert's problems to solve for a MGA mission. |

| | |
|---|---|
| $N_{particles}$ | Number of particles in the PSO algorithm swarm. |
| $N_{variables}$ | Number of decision variables to be optimized via PSO algorithm. |
| $\vec{\omega}_{\oplus}$ | Angular velocity vector of Earth's body-fixed frame. |
| $\phi,\ \psi$ | Arbitrary unknown decision variables in PSO algorithm. |
| $\hat{p}$ | Primary axis of perifocal frame, pointing to periapse location of orbit. |
| $\mathbf{p}_{Best,G}$ | Global best "position" for particle within PSO algorithm. |
| $\mathbf{p}_{Best,j}$ | Personal best "position" for particle within PSO algorithm. |
| $\mathbf{p}_j$ | The "position" for an individual particle within PSO algorithm. |
| $\mathbf{p}_j^*$ | Update to the "position" for an individual particle within PSO algorithm. |
| PDS | NASA's Planetary Data System. |
| PRCF | Planetocentric Rotating Coordinate Frame. |
| PSO | Particle Swarm Optimization. |
| $\hat{q}$ | Third axis of perifocal frame, completing a right-handed set. |
| $r$ | Magnitude of position vector, two-body problem. |
| $\vec{r}$ | Position vector, two-body problem. |
| $r_0$ | Magnitude of initial position vector, Lagrange coefficients. |
| $\vec{r}_0$ | Position vector at epoch time, Lagrange coefficients |
| $\vec{r}_1$ | Position vector on initial orbit, starting position vector on transfer orbit, Lambert's problem. |
| $\vec{r}_2$ | Position vector on final orbit, ending position vector on transfer orbit, Lambert's problem. |
| $r_1(0,1)$ | Random number for inertial acceleration coefficient using uniform distribution from 0 to 1 |
| $r_2(0,1)$ | Random number for cognitive acceleration coefficient using uniform distribution from 0 to 1 |

| | |
|---|---|
| $r_3(0,1)$ | Random number for social acceleration coefficient using uniform distribution from 0 to 1 |
| $r_a$ | Radius of apoapse, two-body problem. |
| $r_p$ | Radius of periapse, two-body problem. |
| $r_p^-,\ r_p^+$ | Radius of periapse into flyby planet, out of flyby planet, synergetic flyby. |
| $r_{p,min}$ | Minimum acceptable radius of periapse at flyby encounter of a planet. |
| $r_{SOI}$ | Radius of Sphere of Influence. |
| $R_{FB}$ | Planetary radius of a flyby planet. |
| $s$ | Seconds of Calendar date. |
| SICF | Sun-centered inertial coordinate frame. |
| SOI | Sphere of Influence. |
| $\theta$ | True anomaly of spacecraft (or object) in orbit, two-body problem. |
| $\theta_0$ | True anomaly at epoch time, Lagrange coefficients. |
| $\theta_\infty$ | True anomaly at infinity along hyperbolic orbit, two-body problem. |
| $\Delta\theta$ | Change in true anomaly, two-body problem. |
| $t$ | Time of interest, two-body problem. |
| $t_0$ | Epoch time, Lagrange coefficients. |
| $t_1$ | Starting time for entrance onto transfer orbit, Lambert's problem. |
| $t_2$ | Ending time for exit from transfer orbit, Lambert's problem. |
| $t_p$ | Time of last periapse passage, two-body problem. |
| $T$ | Period of orbit, two-body problem. |
| $T_{total}$ | Total time of flight for a MGA mission. |
| $TOF_{1to2}$ | Time of flight from flyby encounter 1 (GA 1) to flyby encounter 2 (GA 2) for a MGA mission. |

$TOF_{Lto1}$ Time of flight from launch to flyby encounter 1 (GA 1) for a MGA mission.

$TOF_{N-1toN}$ Time of flight from flyby encounter $N-1$ (GA $N-1$) to flyby encounter $N$ (GA $N$) for a MGA mission.

$TOF_{NtoA}$ Time of flight from flyby encounter $N$ (GA $N$) to arrival for a MGA mission.

$v$ Magnitude of velocity vector, two-body problem.

$\vec{v}_\infty^-$ Hyperbolic excess velocity vector into hyperbolic orbit (flyby), two-body problem.

$v_\infty$ Speed for hyperbolic excess velocity vector, two-body problem.

$\vec{v}_\infty^+$ Hyperbolic excess velocity vector out of hyperbolic orbit (flyby), two-body problem.

$\vec{v}_{sc/\otimes}^-$ Velocity vector of spacecraft with respect to the planet into the flyby encounter.

$\vec{v}_{sc/\otimes}$ Velocity vector of spacecraft with respect to the planet.

$\vec{v}_{sc/\otimes}^+$ Velocity vector of spacecraft with respect to the planet out of the flyby encounter.

$v_0$ Magnitude of initial velocity vector, Lagrange coefficients.

$\vec{v}_0$ Velocity vector at epoch time, Lagrange coefficients.

$\vec{v}_1$ Starting velocity vector on transfer orbit, Lambert's problem.

$\vec{v}_2$ Ending velocity vector on transfer orbit, Lambert's problem.

$\vec{v}_i$ Velocity vector on initial orbit, Lambert's problem.

$\mathbf{v}_j$ The "velocity" for an individual particle within PSO algorithm.

$\mathbf{v}_j^*$ Update to the "velocity" for an individual particle within PSO algorithm.

$v_p^-,\ v_p^+$ Speed at periapse into flyby planet, out of flyby planet, synergetic flyby.

$v_{r0}$ Initial radial velocity component, Lagrange coefficients.

| | |
|---|---|
| $\Delta\vec{v}_1$ | Delta-v to enter transfer orbit, Lambert's problem. |
| $\Delta\vec{v}_2$ | Delta-v to exit transfer orbit, Lambert's problem. |
| $\Delta v_s$ | Magnitude of delta-v required for synergetic flyby. |
| $\lvert\Delta\vec{v}_{s_1}\rvert$, $\Delta v_{s_1}$ | Magnitude of planetocentric delta-v required for synergetic flyby maneuver 1 for a MGA mission. |
| $\lvert\Delta\vec{v}_{s_N}\rvert$, $\Delta v_{s_N}$ | Magnitude of planetocentric delta-v required for synergetic flyby maneuver $N$ for a MGA mission. |
| $\vec{V}_{\otimes/\odot}$ | Velocity vector of planet with respect to the Sun. |
| $\vec{V}^-_{sc/\odot}$ | Velocity vector of spacecraft with respect to the Sun into the flyby encounter. |
| $\vec{V}^+_{sc/\odot}$ | Velocity vector of spacecraft with respect to the Sun out of the flyby encounter. |
| $\lvert\Delta\vec{V}_A\rvert$, $\Delta V_A$ | Magnitude of Sun-centered delta-v required for arrival in a MGA mission. |
| $\lvert\Delta\vec{V}_{FB}\rvert$, $\Delta V_{FB}$ | Magnitude of Sun-centered delta-v required at a flyby encounter in a MGA mission. |
| $\Delta V_{max}$ | Maximum scalar change in velocity with respect to the Sun that can occur for a free-flight flyby encounter (GA) of a given planet. |
| $\lvert\Delta\vec{V}_L\rvert$, $\Delta V_L$ | Magnitude of Sun-centered delta-v required for launch in a MGA mission. |
| $\hat{w}$ | Secondary axis of perifocal frame, co-linear with specific angular momentum vector of orbit. |
| $w_p$ | Weight for periapse violation penalty term (always positive) in cost function for a MGA mission. |
| $\hat{x}$ | Primary axis of PRCF pointing in direction of the planet's velocity vector with respect to the Sun. |
| $\hat{X}$ | Primary axis of SICF pointing in direction of first point of Aries. |
| $\mathbf{X}_0$ | Initial guess for a vector of unknown variables for a multivariate Newton-Raphson scheme. |

$\mathbf{X}_i$ Vector of unknown variables for a multivariate Newton-Raphson scheme.

$\mathbf{X}_{i+1}$ Vector of unknown variables at next iteration for a multivariate Newton-Raphson scheme.

$\hat{X}_{ICRF}$ Primary axis of ICRF pointing in direction of first point of Aries.

$\delta\mathbf{X}_i$ Correction to a vector of unknown variables in a multivariate Newton-Raphson scheme.

$\hat{y}$ Third axis of PRCF completing the right-handed set.

$\hat{Y}$ Third axis of SICF completing the right-handed set.

$\hat{Y}_{ICRF}$ Third axis of ICRF completing the right-handed set.

$yr$ Year of Calendar date.

$\hat{z}$ Secondary axis of PRCF pointing in direction of the orbit's specific angular momentum vector with respect to the planet.

$\hat{Z}$ Secondary axis of SICF pointing in direction of Earth's orbit-normal with respect to the Sun.

$\hat{Z}_{ICRF}$ Secondary axis of ICRF pointing in direction of the Earth's spin axis.

# Acknowledgments

I would like to extend the most sincere thank you to my parents Michael and Mary Ann Shaw for their love and support throughout my graduate education. I appreciate their patience and encouragement. I would also like to thank my sister Megan Shaw, for her love and support. When I decided to enter graduate school, I found myself entering uncharted territory for a member of my family. Nothing makes me more comfortable as a student than to have their constant positive encouragement day in and day out. Even on days when things did not go my way, my family was always there to pick me up and dust me off.

Thank you to some of my role models throughout my life. Uncle Joe, you have always demonstrated for me that a path into the unknown is not something to fear, but to embrace. For that, I will always admire you. I hope to blaze my own trail in my life much like you have for yours. Paul Dirling, thank you for constantly teaching me to be humble throughout my life. I've learned so much from you, and owe a great deal of the skills for patience and teaching that I've acquired over time to you (and of course some of them to Mike Shaw too).

Next I want to extend my gratitude to my best friends at home in Pittsburgh, those friends in Happy Valley, and the friends who have traveled far away from either of those places in order to chase their dreams. Your perspectives on life have always provided me with optimism, companionship, and reliability throughout my journey to become an Aerospace engineer.

Veronica, thank you for your constant love and partnership throughout my graduate career. I certainly would have been lacking in so much that life has to offer if you were not by my side the whole way.

Thank you to those student mentors and colleagues that have shaped my graduate career. Sarah, thank you for your mentor-ship throughout the process of writing my thesis. Thank you to two of my closest friends at Penn State, Chris and Rachel for your positive attitudes and wonderful outlook on life the past two years. Thank you to the research colleagues in the 306 Engineering Unit B office that have provided ideas and constructive feedback throughout the process of learning what it is like to be a graduate researcher.

I want to thank those within the Aerospace Engineering Department who have shaped my education and career path in such profound ways. First, I must acknowledge my advisor Dr. Melton for his phenomenal support, care, and for shaping me as a graduate student and a person. It has been an honor to work under a role model in the Aerospace field, and to see such a gifted teacher both in classroom and behind the scenes. I hope that one day I can be a professor with as much respect, candor, and passion for education as you have had when teaching some very fortunate Penn State students. To Dr. Maughmer, thank you for your unofficial advising, your honest opinions, and helping make me a stronger and more intelligent person. Dr. Spencer, thank you for serving as a dependable mentor in my professional and educational career, and helping me obtain a solid foundation for this research through so many quality astrodynamics courses.

I would like to thank two people from John's Hopkins Applied Physics Lab (APL) for helping me directly with research progress. Christopher Scott, thank you for helping steer me towards some great background material on gravity assist tour designs. Marty Ozimek, thank you for sharing a dependable Lambert solver program in MATLAB with Penn State's astrodynamics research group that I used directly in my research.

Finally, I would like to acknowledge and extend a sincere thank you to the NASA Pennsylvania Space Grant Consortium for their financial support in the form of a fellowship to conduct the research presented in this thesis. The financial support has made my research possible and enriched my education as a whole.

# Chapter 1
# Introduction

## 1.1 Background

Travel to distant places within the solar system is exciting, adventurous, and also valuable to scientific discovery and inquiry. In the past, missions such as Voyager, Cassini-Huygens, and Galileo (to name only a few) have made fundamental discoveries and contributed to scientific advancement in unique ways. However, the results and findings from these missions were obtained by use of unique trajectories that required more than one gravitational assist maneuver (GA) between Earth and the arrival destination of choice. A gravitational assist is an event where a spacecraft receives a change in velocity with respect to the Sun due to an exchange of angular momentum from flying close to another body in the solar system. Therefore, each time the spacecraft of Voyager 1, Voyager 2, or Cassini needed a significant change in velocity the boost came by flying close to a nearby planet. The flyby encounters allowed the spacecraft to receive a delta-v that might otherwise be impossible. In fact, these trips are often so difficult that they ordinarily could not have been executed in the absence of gravitational assist maneuvers. The propellant required to visit outer gas giants and some of the inner neighbors to the Earth often exceeds the largest tank capacity that is technologically possible. Much research into advanced propulsion techniques continues in the hopes of expanding the types of feasible missions for which future spacecraft can be designed.

For now though, limitations on propellant are very constraining and often limit many aspects of missions. For example, the decision to carry enough propellant for a given mission outweighs the desire to carry extra scientific payloads in most cases. Other times, mission trajectories would not be possible within a desired schedule if it were not for the use of gravitational assists [3].

The gravitational assist was first analyzed and proposed by Minovitch [4] while

he was a researcher at UCLA and JPL. The reliability of the gravitational assist has been proven in past missions for achieving otherwise unattainable goals. The use of the gravity assist maneuver allows for everything from customizing science surveys of other planets to accommodating changes to mission plans on the fly, by extending mission lifetime through propellant savings. Additionally, a gravity assist maneuver called a synergetic gravity assist offers more benefits. These flybys involve a man-made engine burn from a spacecraft in combination with a gravity assist maneuver (also known as a powered flyby [5]). The consideration of such a maneuver expands the interplanetary trajectory options for mission designers, by opening up more transfer orbit possibilities between planets.

Overall, the large number of capabilities comes with a price. The planning of trajectories involving more than one gravitational assist remains a daunting task. Planets have special phasing regarding relative positions with one another that plays a key role in determining the cost of a trajectory in terms of propellant. Mission designers must somehow consider non-intuitive factors for phasing that add complexity to missions. Often, the best solutions require encounters along the way that may not be expected at first glance. Further, determining the perfect time to take one trajectory over another is not obvious for most mission cases. Therefore, this area of research has challenged many engineers in the past.

## 1.2 Gravity Assist Maneuver Literature

Identification of optimal interplanetary trajectories that involve more than one gravitational assist has attracted much attention from space flight researchers. Many algorithms and approaches have been applied in order to gain some insight into the problem with the hopes of finding the best trajectories available for less computational expense.

Many have conducted research in the past to identify the number of gravitational assists that a trajectory should use, what times are best for those given flyby encounters, and how the previous two conditions affect one another (to further complicate the problem). Through previous work, it is well understood that there are multiple optimization problems available to solve, but no researcher or group has found a method that is capable of guaranteeing globally optimal results. The broader optimization problem for multiple gravity assists is determining the optimal number of flyby encounters for a given mission and which bodies to target for

those flyby encounters, and is referred to as the sequencing problem. Additionally, the solution to the sequencing problem is undoubtedly affected by a narrower optimization problem. The narrower optimization problem is to determine which dates the flybys within a sequence should occur on, and is referred to as the scheduling problem. This thesis addresses the scheduling problem with a new approach.

Trajectories that were designed in the past, for missions such as Galileo and Cassini [6, 7], used solution approaches solving the sequencing and scheduling problem together, with less automation than today's methods. Often, humans played a key role in the design loop, which meant looking at the trade-space for the design of a trajectory took long periods of time. Further, there is the consequence of missing an optimal solution if not enough cases are evaluated.

Often, research has focused on the sequencing problem by trying to identify better methods to evaluate options for the sequence of planets that are to be visited, and potentially the number of planets. This portion of the multiple gravity assist problem is frequently compared to a traveling salesman problem. In general, the traveling salesman problem refers to a problem involving scheduling of some type of action, task, or perhaps destinations along a travel schedule. A start condition and end condition are known ahead of time, but the number of conditions or order of conditions required between the start and end may both be free for selection. Here, the problem pertains to selections for flyby encounters in a multiple gravity assist trajectory. The number of flybys, as well as the sequence of planets to encounter are both unknown. However, each sequence then contains a set of flyby choices. The first flyby choice will directly shape the options available for all future flyby opportunities in the solution. Due to this relationship, often it becomes desirable to consider all possible choices by evaluating solutions in a tree-search structure. Each choice represents a fork in a tree-branch, where all paths (branches) are considered and evaluated. Once the arrival destination is reached for each branch, the permutations are all evaluated side by side in order to determine the optimal solution. This can quickly become a daunting piece of analysis for missions that involve several gravitational assists.

If a sequence of planets that a mission will encounter is considered as known, then the problem becomes a pure scheduling one. The determination of flyby dates is conventionally found by an incremental solution approach starting at the launch location and aiming towards the arrival destination by solving for the

discrete known free-flight flyby encounters one by one, sequentially. The problem here is that although the planets and their order of visitation are set, the options chosen for flyby encounters still has a deterministic relationship. A downfall with this approach is that there is no guarantee that a flyby choice made for the first planetary encounter will actually provide a solution that ends at the proper arrival location. Again, the flyby date made for the first planet directly affects all choices available at future flyby encounters in this way. Vasile et al [8] recently revisited this type of approach in an effort aimed at automating the design process for these trajectories versus older methods that involved human decision making in the design process. However, as the number of flybys considered for the scheduling problem between launch and arrival increases (or is changed as part of the trade-space), the incremental approach quickly proves to be computationally overwhelming, even for modern computing systems. Due to these computational challenges, other research has focused on transcribing the problem into a different viewpoint in the hopes of limiting the computational expense [9].

Some of the most successful approaches to date has been those that have split the problem into two separate treatements, one for the scheduling problem and one for the sequencing problem. One of the most effective approaches for the scheduling problem remains that taken by Longuski [10]. Graphical methods were demonstrated by Strange and Longuski [11] as promising directions to research for the planetary sequencing problem. By contrast, Izzo [12] reduced the search space for the multiple gravity assist problem as a whole without separate treatments, and showed some initial advantages that heuristic algorithms have for reducing the computational load of the problem. Other approaches involve a multi-objective optimization using non inferiority and smallest loss criterion [13], a method of virtual trajectories [14], and a multi-variable nonlinear iterative approach [15].

Hybrid approaches have also been investigated for both the scheduling and the sequencing problems, with focus on combining complementary algorithms in order to get the best benefits from each method to work together in unison. Genetic algorithms in combination with a local search method using recursive quadratic programming was investigated in 2000 [16]. In 2015, a combination between genetic algorithms and nonlinear programming gradient-based optimization was researched [17]. Other researchers have recently examined a breadth-first search (BFS) algorithm that also involves a differential evolution variant [18]. The research community is interested in looking towards heuristic methods for optimization of

either the scheduling or sequencing problem. One particular heuristic approach that has has proven attractive for peripherally related problems in space flight mechanics research is Particle Swarm Optimization (PSO).

## 1.3 Particle Swarm Optimization in Space Flight Mechanics

The use of Particle Swarm Optimization (PSO) is not exclusive to the field of space flight mechanics. The algorithm is a heuristic approach to optimization that was first developed in 1995 for use in nonlinear function optimization [19]. Since its first appearance, the method has found its way into the realm of space flight mechanics for solving many different types of problems. Bessette [20] and Bessette and Spencer [21] showed that PSO has encouraging behavior and performance on a trajectory optimization problem involving one gravitational assist maneuver. As part of the future work discussed there, research into PSO's performance on a multiple gravity assist problem was recommended. Pontani and Conway [22] showed that PSO had promise for solving other types of orbital mechanics problems, such as simple two body transfers, low-thrust trajectories, and the restricted three-body problem. In addition to these applications, PSO has recently been applied to problems involving re-entry trajectories [23, 24]. Additional interplanetary research involving PSO was conducted for trajectories from Earth to outer planets with consideration of optimal propellant solutions as well as multi-objective solutions in both minimal propellant and minimal time [25]. PSO has recently helped identify optimal slewing paths for attitude dynamics problems involving constraints [26]. The scheduling problem associated with multiple gravity assist trajectories appears to be a suitable candidate for the application of Particle Swarm Optimization (PSO).

## 1.4 The Problem and an Approach to Solution

The scheduling problem is one that involves selecting the dates of flyby encounters (continuous variables) for a multiple gravity assist trajectory. This thesis presents a solution approach to the scheduling problem, and will refer to this problem as the multiple gravity assist (MGA) problem hereafter. For each mission examined in this thesis, a sequence of planets for flyby encounter(s) is assumed as known, and their order remains fixed. The solution to this problem is a sequence of

sun-centered orbits that allows a spacecraft to travel from Earth to an arrival destination planet subject to flyby(s) of other planets in between. The solution approach is first executed on the well known multiple gravity assist trajectories from the past missions Voyager 1, Voyager 2, and Cassini for verification against their real-life flyby dates. After verification, the method is then applied to a novel mission design case. This mission design case is compared to a direct route from launch planet to arrival planet where no gravity assist maneuvers are involved.

The new solution approach is threefold. First, a new formulation for synergetic (powered) flyby encounters is derived and implemented for the scheduling problem in order to expand the number of feasible interplanetary trajectories that are possible. Second, a new formulation for the scheduling problem is created in terms of a multivariate optimization problem. Here, the optimal solution is viewed as one that requires the least amount of propellant and does not pass within a flyby planet's radius. Lastly, new methods to thoroughly investigate the MGA problem search space in less computational time are still of interest to the research community. This thesis applies the Particle Swarm Optimization (PSO) optimization algorithm to demonstrate its computational efficiency when identifying optimal trajectories for interplanetary travel. The method of this thesis provides a key advantage versus previous methods. The approach to solution presented here allows for quick determination of an optimal interplanetary trajectory for a mission without the need for human intervention at each flyby, as with past design processes. Further, it expands upon the normal considerations for gravity assists by allowing synergetic flyby maneuvers instead of purely free-flight ones. This change to the normal methods for the scheduling problem eliminate the issue where solutions do not meet the desired arrival conditions. Every solution that is evaluated by PSO is a solution that arrives at the desired arrival planet, the only consequence is that some of these solutions may require large and unrealistic amounts of propellant. Although this seems to be potentially problematic, the propellant cost can then serve as a direct measure of the "goodness" for a given solution. Ultimately, PSO has been selected for this research due to its robustness in identifying the best solutions for multi-variable optimization problems framed in this way.

## 1.5 Governing Research Questions

With much research conducted in areas either directly related to multiple gravity assist trajectory design or peripherally related to the topic, it is important to identify the questions that this research seeks to provide answers to:

**Question 1:** How does Particle Swarm Optimization perform for the multiple gravity assist trajectory design space?

**Question 2:** What benefits and downfalls exist when formulating the scheduling problem for gravitational assist maneuvers as a multivariate optimization problem minimizing propellant?

**Question 3:** Can previous mission results be either confirmed or improved using this approach?

# Chapter 2
# Orbital Mechanics Background

The design of a multiple gravity assist mission trajectory requires a mastery of a combination of fundamental concepts from orbital mechanics. The most critical fundamental concepts that are required in order to develop the solution method presented in this thesis are gathered for the reader in this chapter. Though this chapter seeks to clarify what concepts are crucial and how they were applied to the MGA problem, some familiarity with the two-body problem and related principles are assumed of the reader. If further clarification is necessary, some helpful resources that approach the principles from unique perspectives are texts by Vallado [27], Bate, Mueller, and White [28], Prussing and Conway [29], Curtis [1], Walter [30], and Wiesel [31]. A much more in-depth text that covers specifically the math and physics of multiple gravity assist trajectories is that of Labunsky, Papkov, and Sukhanov [2].

## 2.1 The Two-Body Problem

The two-body problem is a classical starting point for any analysis in orbital mechanics. The dynamic model is commonly studied in preliminary mission design because of its simplicity as compared to the full dynamics that spacecraft are subject to in real-life operation. The details are often good enough for a first cut at mission design, especially in the context of interplanetary travel. The two-body problem is the governing dynamic model for the work of this thesis.

In two-body dynamics, the assumption is made that the central body is the most massive of all objects involved. As a consequence of this assumption, the mass of the orbiting body is neglected as very small with respect to the central body. For example, the mass of each planet (even Jupiter) is neglected when modeling the orbit of each planet around the Sun, without loss of much detail. Similarly, the

mass of a spacecraft is considered very small with respect to the Sun, and is also neglected. Even the orbit of the spacecraft with respect to a planet is captured with acceptable detail by neglecting the mass of the spacecraft itself.

Another key characteristic of the two-body problem is that its solution exclusively applies to Keplerian orbits, i.e. orbits that obey Kepler's three laws.

1. The planets and their orbits follow elliptical paths with the Sun at one focus.
2. The planets and their orbits sweep equal areas in equal times (directly relating to conservation of angular momentum).
3. The square of the period of a planet's orbit is proportional to the cube of the orbit's semi-major axis.

Additionally, the term Keplerian is reserved to describe orbits which are free of all perturbation effects. Such effects that in reality perturb a two-body Keplerian orbit are the gravitational effects of additional bodies on a trajectory (often termed the $N$-body problem), solar radiation pressure (accumulated as a force over area for the body of the spacecraft), or atmospheric drag (for orbits that fly close enough to planetary atmospheres to warrant this consideration). The differential equations (equations of motion) that describes the typical motion of an object orbiting a central body in the two-body problem are:

$$\ddot{\vec{r}} = -\frac{\mu \vec{r}}{r^3} \tag{2.1}$$

where $\mu$ is the central body's gravitational parameter, and $\vec{r}$ is the position vector of the orbiting body in an inertial frame. The possible orbit types that satisfy these differential equations are given by conic sections. The practical conic section orbits are circles, ellipses, parabolas, and hyperbolas. The circular and parabolic orbits are not themselves observed in real-life, but instead serve as mathematical constructs to understand the bridge between closed orbits (circles and ellipses) and open orbits (parabolas and hyperbolas). In fact, the circle can be thought of as a special case of the ellipse and the parabola can be viewed as a special case of the hyperbola.

## 2.2 Analytic Solutions

The solution to Eq. (2.1) is known as the orbit equation. Any trajectory that is a solution to Eq. (2.1) is an orbit that lies within a plane. This unique plane contains all of the motion of the orbiting body with respect to the central body, and is called the orbital-plane.

A unique coordinate system is developed to describe the trajectory given by the orbit equation in a convenient reference frame. The perifocal reference frame is inertial, and easily facilitates tracking the motion of the orbiting body in its native orbital-plane. The origin of the perifocal frame is the focus $F$, or the center of the central gravitational body. The primary axis is $\hat{p}$ and points in the direction of periapse (closest point on the orbit to the central body). The secondary axis $\hat{w}$ is co-linear with the orbit-normal direction (the specific angular momentum vector for the orbit). The $\hat{q}$ axis is chosen to complete the right-handed set and lies within the orbital plane. An illustration of the perifocal reference frame and the possible solutions to the orbital equations of motion are included in Figure 2.1.

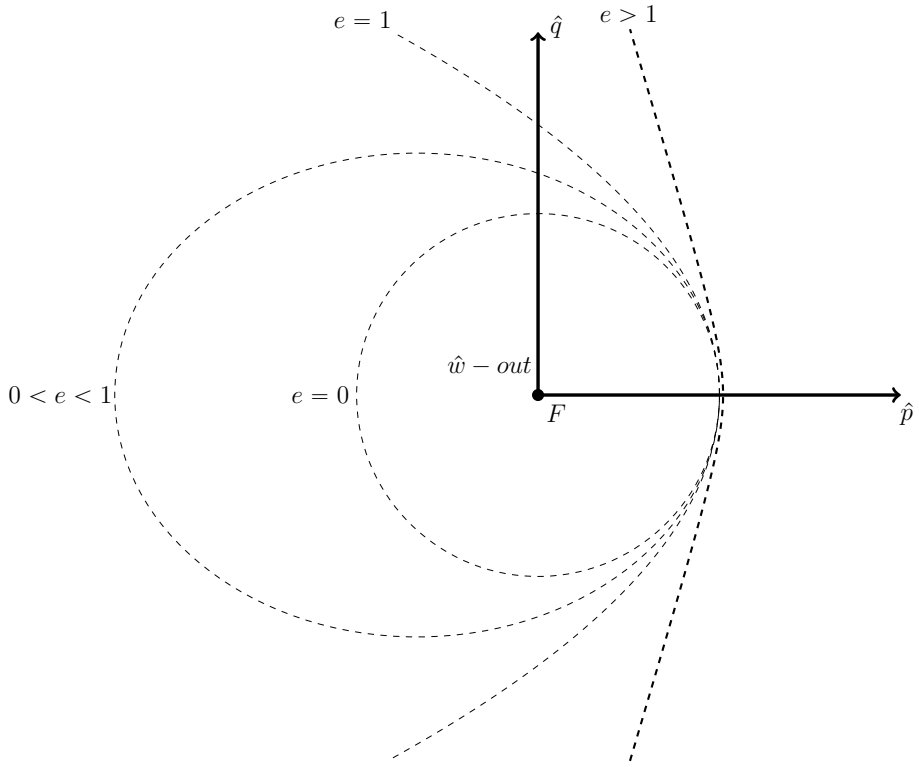


Figure 2.1: Circular orbit ($e = 0$), elliptical orbit ($0 < e < 1$), parabolic orbit ($e = 1$), and hyperbolic orbit ($e > 1$) solutions in the perifocal frame.

The orbit equation describes the relationship between the position vector's magnitude and its angular position away from the primary $\hat{p}$ axis. Time is an implicit variable in this sense, and the angle swept out is referred to as the true anomaly, denoted by $\theta$. The orbital position is a function of the orbit's geometric properties:

$$r = \frac{a\,(1 - e^2)}{1 + e\cos\theta} \tag{2.2}$$

where $e$ is the eccentricity and $a$ is the semi-major axis of the ellipse. Beware, as different authors may adopt different symbols to describe the true anomaly. Similarly, there are multiple acceptable forms of the orbit equation in terms of other geometric orbital parameters.

An additional fundamental principle to orbital mechanics is the conservation of energy. The conservation of energy as applied to orbital mechanics involves specific energy, and has been named the vis-viva equation (Latin for living force):

$$\frac{v^2}{2} - \frac{\mu}{r} = -\frac{\mu}{2a} \tag{2.3}$$

The relationship for the vis-viva equation is applicable to all points in an orbit along all types of conic sections. The relationship for energy balance can be used to determine scalar velocity (speed) at a point on the orbit where the scalar position is known.

### 2.2.1 Elliptical Orbits

Elliptical orbits are closed in nature, and in this way describe the motion of all planets within the solar system. General geometry for an elliptical orbit is presented in Figure 2.2. The value of the eccentricity is between $0 < e < 1$ for elliptical orbits (circular orbits are $e = 0$) and determined as:

$$e = \frac{r_a - r_p}{r_a + r_p} \tag{2.4}$$

where the closest point to the central body is the periapse radius:

$$r_p = a(1 - e) \tag{2.5}$$

and farthest point from the central body is the apoapse radius:

$$r_a = a(1 + e) \tag{2.6}$$

The perifocal frame is placed at the occupied focus ($F$) where the central body is located. The empty focus ($F'$) is purely geometric in nature, and does not hold any central mass or body contributing to dynamics. The occupied focus and the vacant focus both lie on a line known as the line of apsides (LOA). For the case of a circular orbit, the occupied focus and the vacant focus lie on top of one another at the center of the circle.

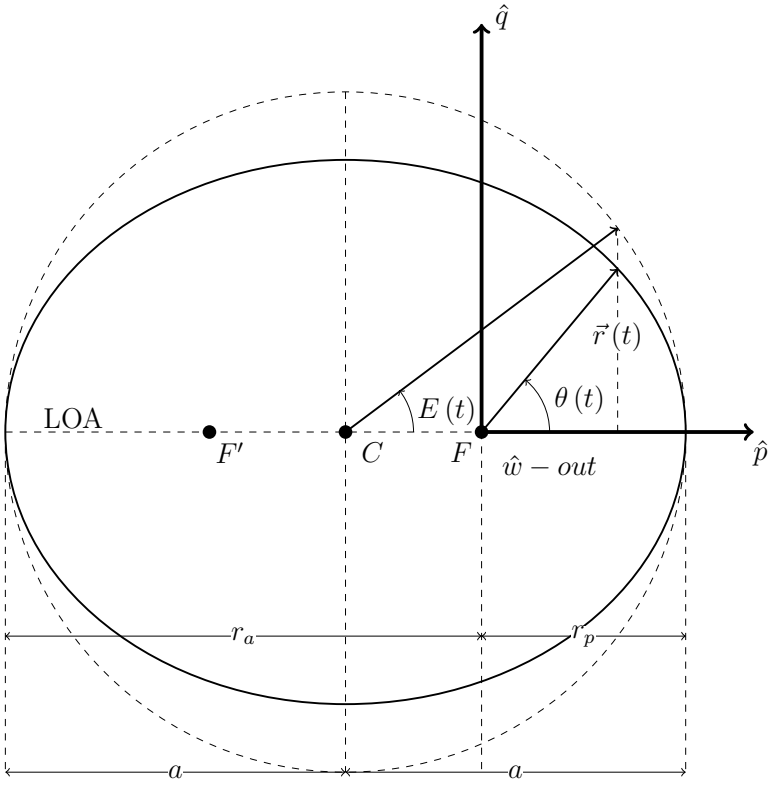


Figure 2.2: The geometry for an elliptical orbit (solid) and the auxiliary circle (dashed).

Calculations involving the motion of a spacecraft traveling on an elliptic orbit are related to the geometry of the orbit as well as the mass of the gravitational center. The motion of a spacecraft around the central body is propagated through time by Kepler's time equation:

$$M = n(t - t_p) = E - e \sin E \tag{2.7}$$

where $M$ is the mean anomaly of the orbit, $n$ is the mean motion in radians per second found by:

$$n = \sqrt{\frac{\mu}{a^3}} \tag{2.8}$$

the time since last periapse passage is $(t - t_p)$, and $E$ is known as the eccentric anomaly. The eccentric anomaly is determined by circumscribing an auxillary circle around the elliptical orbit. Tracking of a given position on the orbit is directly

related to tracking a corresponding position on the auxillary circle by the half-angle relationship:

$$\tan\frac{E}{2} = \sqrt{\frac{1-e}{1+e}}\tan\frac{\theta}{2} \tag{2.9}$$

If a time of flight is known, then Kepler's equation can be solved directly for the future position of a spacecraft or orbiting body in an orbit with known geometric properties. However, the solution for determining the time of flight from one position on a known orbit to another position on a known orbit is iterative in nature, due to the transcendental nature of Eq. (2.7). A common and successful method to solve the equation is found via Newton-Raphson iteration scheme for eccentric anomaly:

$$E_{i+1} = E_i - \frac{f(E_i)}{f'(E_i)} \tag{2.10}$$

where

$$f(E_i) = E_i - e\sin E_i - M \tag{2.11}$$

and

$$\frac{df(E_i)}{dE_i} = f'(E_i) = 1 - e\cos E_i \tag{2.12}$$

Here, the eccentric anomaly is first assumed as the value of the mean anomaly:

$$E_0 = M = n(t - t_p) \tag{2.13}$$

Iterative approach is used to evaluate Eqs. (2.10-2.12) until the value of the difference in eccentric anomaly between two respective iterations is below some user-specified absolute tolerance (note: a relative tolerance could also be used):

$$|E_{i+1} - E_i| \leqslant \Delta_A \tag{2.14}$$

Lastly, the time it takes a spacecraft or body to complete one orbit is known as the period of the orbit and is given as Kepler first suggested in his third law:

$$T = 2\pi\sqrt{\frac{a^3}{\mu}} = \frac{2\pi}{n} \tag{2.15}$$

### 2.2.2 Hyperbolic Orbits

Hyperbolic orbits are open in nature, and in this way are most useful to describe the motion of spacecraft as it encounters planets while traveling on its orbit around the Sun. This occurs when the spacecraft transitions from an orbit exclusively about the Sun to one about a planet.

General geometry for a hyperbolic orbit is presented in Figure 2.3. The value of the eccentricity is $e > 1$ for hyperbolic orbits (parabolic orbits are $e = 1$). The semi-major axis of the orbit is defined as $a < 0$ for the purposes of this thesis, however readers should be aware that alternative descriptions in literature may use a definition of $a > 0$. Both are equally valid, as long as all hyperbolic two-body relations account for the difference in sign.

In the case $a < 0$, the same two-body equations for elliptical orbits are applicable to hyperbolic ones. However, there is no physical apoapse point on a hyperbolic orbit (only a mathematical one) because it is open in nature.

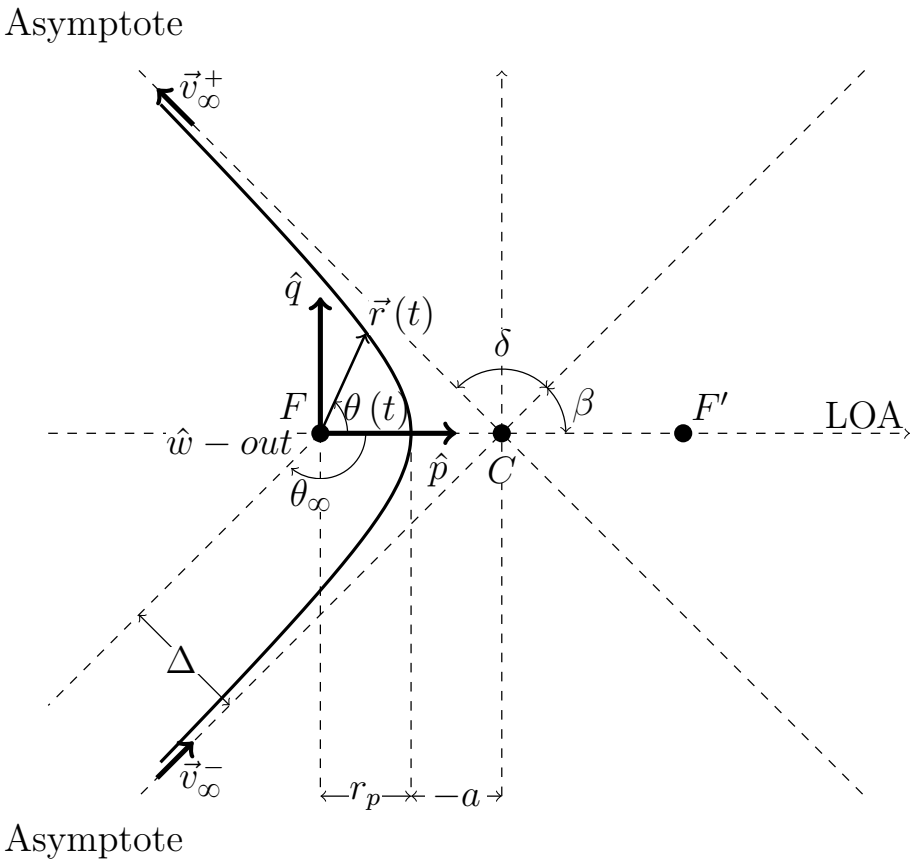


Figure 2.3: The geometry of a hyperbolic orbit.

Key parameters to hyperbolic orbits are the true anomaly at infinity:

$$\theta = \arccos\left(-\frac{1}{e}\right) \tag{2.16}$$

the scalar velocity at infinite radius, known as the hyperbolic excess velocity, can be found from the vis-viva as:

$$v_\infty = \sqrt{-\frac{\mu}{a}} \tag{2.17}$$

the aiming radius, sometimes referred to as impact parameter:

$$\Delta = a\sqrt{e^2 - 1} = r_p\sqrt{\frac{e+1}{e-1}} \tag{2.18}$$

and the turning angle of the hyperbolic trajectory about the central body is:

$$\delta = \pi - 2\beta = 2\arctan\left(\frac{\mu}{\Delta v_\infty^2}\right) = 2\arcsin\left(\frac{1}{e}\right) \tag{2.19}$$

where $\beta$ is the angle between the asymptote that is co-linear with the velocity at infinite radius and the line of apsides for the orbit.

Kepler's time equation is altered to accommodate hyperbolic orbits:

$$M = n(t - t_p) = e\sinh H - H \tag{2.20}$$

where the hyperbolic anomaly is defined as $H$. For the purposes of determining the time it takes an object to fly to a desired point a hyperbola, the true anomaly must be first converted to the hyperbolic anomaly via half-angle relation:

$$\tanh\frac{H}{2} = \sqrt{\frac{e-1}{e+1}}\tan\frac{\theta}{2} \tag{2.21}$$

Analogous to the elliptical case, an iterative Newton-Raphson approach can be used to determine orbital position as a function of time of flight:

$$H_{i+1} = H_i - \frac{f(H_i)}{f'(H_i)} \tag{2.22}$$

where

$$f(H_i) = e\sinh H_i - H_i - M \tag{2.23}$$

and

$$\frac{df(H_i)}{dH_i} = f'(H_i) = e\cosh H_i - 1 \tag{2.24}$$

Here, the eccentric anomaly is assumed as the value of the mean anomaly (just as in the elliptical case):

$$H_0 = M = n(t - t_p) \tag{2.25}$$

Iterative approach is used to evaluate Eqs. (2.22-2.24) until the value of the difference in hyperbolic anomaly between two respective iterations is below some user-specified absolute tolerance:

$$|H_{i+1} - H_i| \leqslant \Delta_A \tag{2.26}$$

## 2.3 Free-Flight Gravitational Assists

A free-flight gravitational assist is a dynamic effect that changes the direction and magnitude of a spacecraft's velocity vector with respect to the Sun under a special circumstance.

In this special circumstance, the spacecraft encounters a nearby third-body, in most cases a planet. The presence of this third-body is called a third-body effect, and this alters both the planet's orbit and the spacecraft's orbit with respect to the Sun. Due to the fact that both the spacecraft and the planet are in orbit around the Sun, no energy is lost or gained with respect to the Sun system as the two encounter one another. However, the planet and spacecraft engage in an elegant exchange of their angular momenta with respect to the Sun. The exchange happens as the spacecraft slingshots around the planet in the planetocentric reference frame and the planet transfers some of its angular momentum with respect to the Sun to the spacecraft. The planet's orbit with respect to the Sun is largely unaffected, due to its mass being much larger than that of a spacecraft. However, as a result of the encounter the spacecraft receives significant change to its dynamics with respect to the Sun.

The main consequence for a free-flight gravity assist is a significant change to the spacecraft velocity direction and magnitude in the Sun-centered reference frame. As the spacecraft encounters the flyby planet, it also encounters the gravitational influence of the flyby planet. The region with which the gravitational influence of a planet supersedes the gravitational influence of the Sun is known as the Sphere of Influence (SOI). As the spacecraft enters the SOI, it travels on a hyperbolic orbit with respect to the flyby planet. Once the spacecraft exits the planet's SOI, the trajectory is assumed to again return to one orbiting the Sun as the primary gravitational source (often elliptical).

Each planet has a unique SOI radius, which can be found in Table 3.1. The SOI value depends largely on the mass of the planet and the distance of the planet from the Sun. Once the spacecraft enters the SOI, the coordinate frame changes from a Sun-centered reference frame to a planetocentric reference frame. A transformation in velocity is easily found by vector subtraction:

$$\vec{v}^{-}_{sc/\otimes} = \vec{V}^{-}_{sc/\odot} - \vec{V}_{\otimes/\odot} \tag{2.27}$$

where the hyperbolic excess velocity into the flyby encounter is $\vec{v}^{-}_{sc/\otimes}$, the spacecraft

velocity before flyby encounter with respect to the Sun is $\vec{V}_{sc/\odot}^{-}$, and the flyby planet's velocity with respect to the Sun is $\vec{V}_{\otimes/\odot}$.

The magnitude of $\vec{v}_{sc/\otimes}^{-}$ is the hyperbolic excess velocity vector magnitude into the flyby encounter in the two-body problem:

$$|\vec{v}_{sc/\otimes}^{-}| = v_{\infty}^{-} = v_{\infty} \tag{2.28}$$

As a result of the flyby encounter, the hyperbolic excess velocity vector magnitude does not change. Consequently, only the direction of the hyperbolic excess velocity vector changes in the planetocentric reference frame. The hyperbolic excess velocity vector into the flyby encounter, $\vec{v}_{sc/\otimes}^{-}$, is effectively turned through the turn angle $\delta$ in the planetocentric reference frame. The turning effect is captured by a direction cosine matrix that uses a simple Euler third-axis rotation:

$$\mathbf{C}_3(\delta) = \begin{bmatrix} \cos\delta & -\sin\delta & 0 \\ \sin\delta & \cos\delta & 0 \\ 0 & 0 & 1 \end{bmatrix} \tag{2.29}$$

The outgoing hyperbolic excess velocity vector is then determined by:

$$\vec{v}_{sc/\otimes}^{+} = \mathbf{C}_3(\delta)\, \vec{v}_{sc/\otimes}^{-} \tag{2.30}$$

Ultimately, the hyperbolic excess velocity out of the flyby is then found by vector addition with the planet's velocity vector with respect to the Sun:

$$\vec{V}_{sc/\odot}^{+} = \vec{V}_{\otimes/\odot} + \vec{v}_{sc/\otimes}^{+} \tag{2.31}$$

Note that the magnitude of $\vec{v}_{sc/\otimes}^{+}$ is equal to $v_{\infty}$ because by definition, direction cosine matrices only rotate vectors and cannot apply scaling effects to vectors. An illustration of the free-flight gravitational assist appears in Figure 2.4.

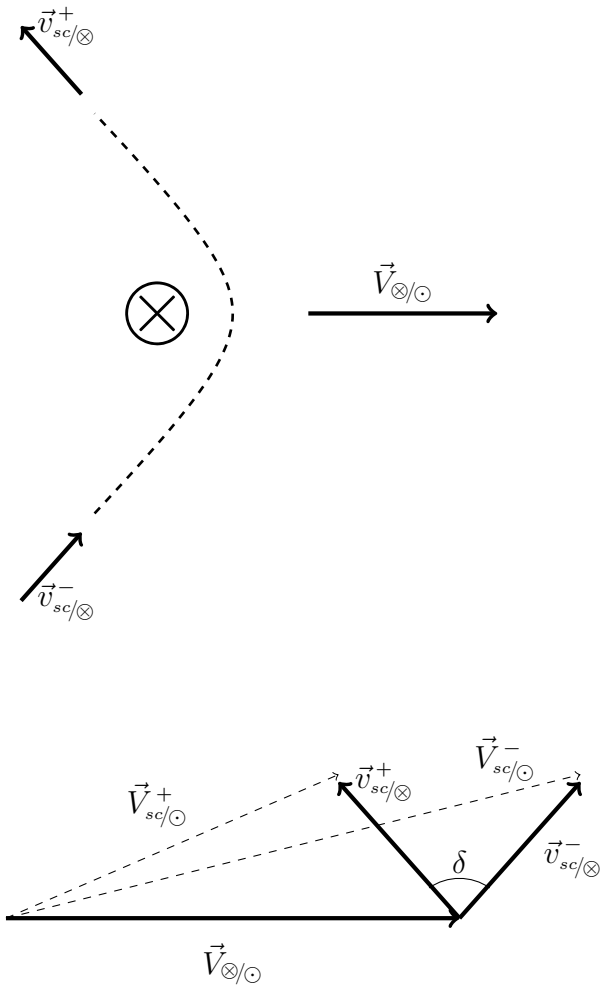


Figure 2.4: The geometry of a free-flight gravitational assist.

Flyby encounters can either increase or decrease the Sun-centered speed of a spacecraft. If a spacecraft encounters the flyby planet from in front of it, then the speed of the spacecraft decreases with respect to the Sun because the planet's perturbation retards the motion of the spacecraft with respect to the Sun (as depicted in Figure 2.4). However, if the spacecraft encounters the flyby planet from behind, then the spacecraft speed with respect to the Sun increases due to the planet's perturbation pulling the spacecraft along with it in orbit around the Sun. Free-flight gravity assist maneuvers can occur around any planet of the solar system (inner or outer). Additionally, other objects can be encountered in this way, such as asteroids or moons belonging to the planets. A smaller, less massive encounter object (such as an asteroid) has a less significant effect on the spacecraft's motion

with respect to the Sun as compared to a much larger, more massive object (such as Jupiter). Overall, the geometry of gravity assist maneuvers is strongly a function of the orientation and magnitude of the velocity vectors coming into and leaving the flyby encounter.

## 2.4 The Julian Date

The idea of timekeeping is one that is critical for space missions. Many different timekeeping methods have been developed for different purposes. The primary method for timekeeping for this research is the Julian date. The concept of the Julian date was first developed in 1582 by Joseph Scaliger, and is a combination of three cycles known as the Roman Indiction, the solar cycle, and the Metonic cycle. The epoch date for this timekeeping method is the shared common point among the three cycles, which happens to be noon on January 1st, 4713 B.C. (a unique singular value) [27].

One reason that the Julian date is such an attractive timekeeping strategy for problems in orbital mechanics is because it allows calendar dates to be displayed in terms of a numerical value. The calculation for determining the Julian date ($JD$) of a given calendar date ($CD = s, min, hr, d, mo, yr$) is:

$$JD = 367\,yr - \text{INT}\left(\frac{7(yr + \text{INT}\left(\frac{mo+9}{12}\right)}{4}\right) + \text{INT}\left(\frac{275\,mo}{9}\right) + d + 1,721,013.5 + \frac{\frac{\frac{s}{60}+min}{60} + h}{24} \quad (2.32)$$

where the INT function represents the real truncation operation [27].

The Julian date allows time to be represented in a continuous mathematical domain, necessary for the application of any continuous-variable optimization methods (including Particle Swarm Optimization). Although all calculation for this research are carried out with Julian dates, the format for presentation in this thesis is always calendar dates.

## 2.5 Coordinate Systems

The basic coordinate systems that are needed in order to carry out calculations and define vectors for this work are the International Celestial Reference Frame (ICRF), the Sun-centered Inertial Coordinate Frame (SICF), and the Planetocentric Rotating Coordinate Frame (PRCF). These coordinate systems all play some role in allowing the location, velocity, or both location and velocity to be defined in a vector sense for different orbital regimes within the MGA problem.

### 2.5.1 International Celestial Reference Frame (ICRF)

The standard coordinate system that all astronomical work and ephemeris data uses is known as the International Celestial Reference Frame. The coordinate frame origin is centered at the barycenter of the solar system. The primary coordinate direction $\hat{X}_{ICRF}$ is placed pointing towards the first point of Aries. The secondary coordinate direction $\hat{Z}_{ICRF}$ is placed in the direction of Earth's spin axis. The third coordinate direction $\hat{Y}_{ICRF}$ completes a right-handed set and lies within the equatorial plane of the Earth. Therefore, the fundamental plane for this coordinate system is the equatorial plane of the Earth. The primary purpose of this coordinate frame is for gathering the ephemerides for all of the planets within the solar system. The angle $\epsilon$ (called the obliquity of the ecliptic) in Figure 2.5 denotes the Earth's equatorial tilt with respect to its orbital plane (called the ecliptic plane) and it is assumed to take a value of 23.5 degrees.

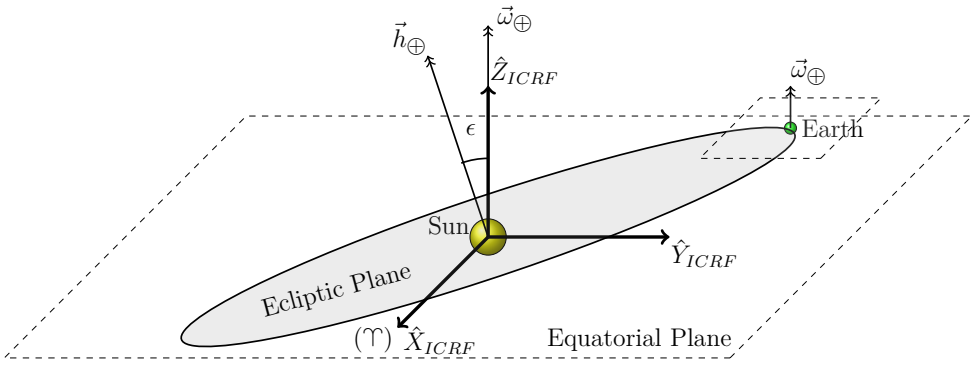


Figure 2.5: International Celestial Reference Frame (ICRF).

### 2.5.2 Sun-centered Inertial Coordinate Frame (SICF)

A natural coordinate system that is common for orbital mechanics work is known as the Sun-centered Inertial Coordinate Frame. This coordinate frame has origin centered at the barycenter of the solar system. For most purposes of preliminary mission design this point is idealized as also being the center of the Sun without much loss of fidelity. In reality, they differ by a finite distance that varies with time as the planets move with respect to the Sun. The location can vary from being almost at the Sun's center to just outside of its surface, depending on the time. The SICF primary coordinate direction $\hat{X}$ is also placed pointing towards the first point of Aries like the ICRF. The secondary coordinate direction $\hat{Z}$ is placed in the direction of Earth's orbit-normal vector, or specific angular momentum vector $\vec{h}_{\oplus}$. The third coordinate direction $\hat{Y}$ completes a right-handed set and lies within the ecliptic plane. A visualization for the SICF is included in Figure 2.6.

There are multiple definitions that are commonly adopted to describe the ecliptic plane (such as the mean orbital plane for all bodies in the solar system). However, this thesis assumes the fundamental plane for the SICF to be Earth's orbital plane for simplicity. The primary purpose of this coordinate frame was for displaying all of the trajectory results presented in this thesis. Velocities of planets are denoted by $\vec{V}_{\otimes/\odot}$, respectively, for this frame. The velocity of the spacecraft is denoted by $\vec{V}_{sc/\odot}$, respectively, for this frame.

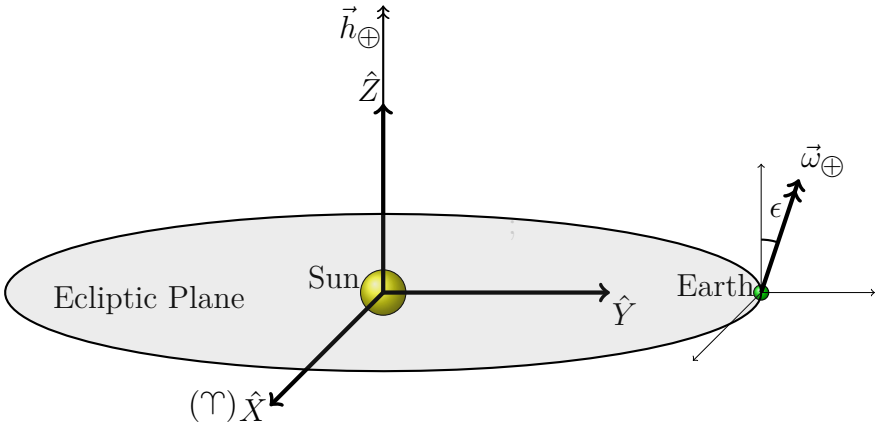


Figure 2.6: Sun-centered Inertial Coordinate Frame (SICF).

In order to obtain vectors in the SICF, a transformation with a direction cosine matrix (DCM) is carried out. The transformation can be viewed as a simple single-axis rotation about the first Euler axis. The DCM that transforms the ICRF

to the SICF is:

$$\mathbf{C}_1(\epsilon) = \begin{bmatrix} 1 & 0 & 0 \\ 0 & \cos\epsilon & \sin\epsilon \\ 0 & -\sin\epsilon & \cos\epsilon \end{bmatrix} \tag{2.33}$$

It is worth noting for clarification that if the orbits of the planets are assumed as co-planar with the Earth's orbit about the Sun, then all planets lie in the ecliptic plane ($\hat{X} - \hat{Y}$ plane). If co-planar orbits are not assumed, then the orbits of all other planets vary slightly in inclination with respect to the $\hat{X} - \hat{Y}$ plane. A table of inclination of the orbits with respect to the ecliptic is given by Table 2.1.

Table 2.1: Orbital inclinations of the planets with respect to the ecliptic plane (data taken from Appendix A of Curtis [1]).

| Planet | Inclination, $i\,(deg)$ |
|---|---|
| Mercury | 7.00 |
| Venus | 3.39 |
| Earth | 0.00 |
| Mars | 1.850 |
| Jupiter | 1.304 |
| Saturn | 2.485 |
| Uranus | 0.772 |
| Neptune | 1.769 |

### 2.5.3 Planetocentric Rotating Coordinate Frame (PRCF)

A final coordinate system that is necessary for the MGA problem is the Planetocentric Rotating Coordinate Frame (PRCF). This coordinate frame has an origin placed at the center of a planet. Each planet has a velocity vector with respect to the SICF, $\vec{V}_{\otimes/\odot}$. The SICF primary coordinate direction $\hat{x}$ is oriented along the velocity vector for the planet, meaning that this coordinate frame is rotating. The secondary coordinate direction $\hat{z}$ is chosen to coincide with the specific angular momentum vector for the trajectory around the planet $\vec{h}_{sc/\otimes}$. The last coordinate direction $\hat{y}$ is oriented as the direction that completes the right-handed set. For eccentric orbits, this means that the $\hat{y}$ axis generally points somewhat away from the Sun line from the planet of interest. If the orbits are assumed as circular, then this axis points directly along the Sun line.

For the MGA problem formulation presented for this research, the vector quantities $\vec{v}^{-}_{sc/\otimes}$ and $\vec{v}^{+}_{sc/\otimes}$ are initially unknown and must be calculated based upon the specifics of the planetary encounter in the SICF. Once the spacecraft enters the planet's SOI, the coordinate frame changes from SICF to PRCF, where a transformation in velocity is easily found into the SOI by Eq. (2.27) and the velocity out of the SOI by rearranging Eq. (2.31):

$$\vec{v}^{+}_{sc/\otimes} = \vec{V}^{+}_{sc/\odot} - \vec{V}_{\otimes/\odot} \tag{2.34}$$

Here, the magnitudes of $\vec{v}^{-}_{sc/\otimes}$ and $\vec{v}^{+}_{sc/\otimes}$ are viewed as hyperbolic excess velocities in a two-body problem, with differing magnitude in general:

$$|\vec{v}^{-}_{sc/\otimes}| = v^{-}_{\infty} \tag{2.35}$$

$$|\vec{v}^{+}_{sc/\otimes}| = v^{+}_{\infty} \tag{2.36}$$

The velocity of the planet with respect to the Sun is idealized as constant through this flyby encounter with an assumption of linked conics (which will be explained in Chapter 3) for the dynamic model. Further, the position of the spacecraft as it moves between the SICF and the PRCF is not required for analysis consistent with a linked conics assumption. Chapter 3 provides insight as to how the velocities $\vec{V}^{-}_{sc/\odot}$ and $\vec{V}^{+}_{sc/\odot}$ are determined. As for the planet velocity, the planetary ephemeris data determines $\vec{V}_{\otimes/\odot}$. Figure 2.7 illustrates this coordinate frame. The primary use of this coordinate frame is to determine trajectory velocities and their scalar speeds for two-body relations. Specifically, we seek the speed of the spacecraft into this frame and out of this frame with respect to the planet as the flyby encounters occur.

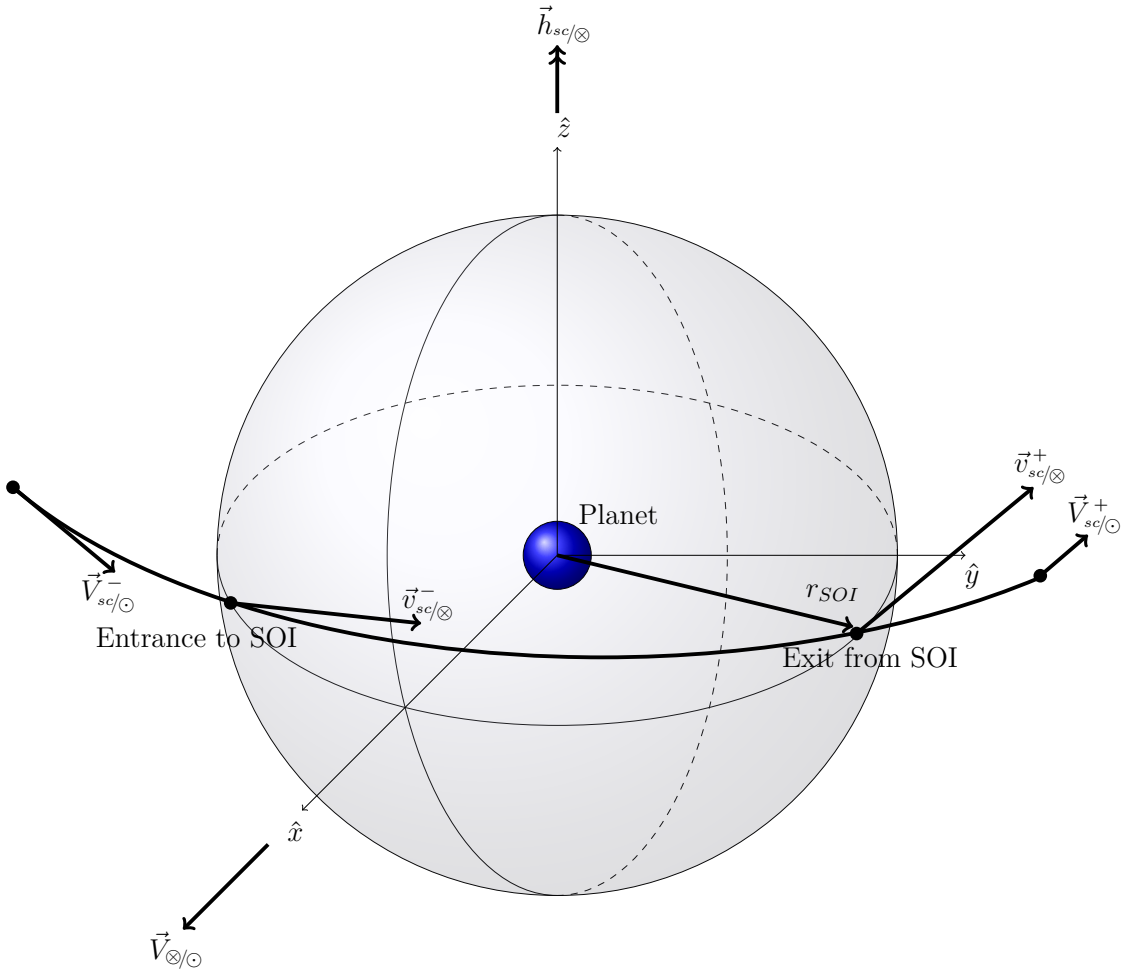


Figure 2.7: Planetocentric Rotating Coordinate Frame (PRCF).

## 2.6 Planetary Ephemerides

The motion of the planets is accounted for at each stage of the MGA problem. In order to properly time a flyby encounter of a planet, the planet's position and velocity must be known with certainty. Classically, the knowledge of position for all of the planets in the solar system was known as the planetary ephemerides. However, the modern meaning of this term has shifted to now indicate both position and velocity of all bodies within the solar system. Further, it is common to refer to the position and velocity of a body as the state of a body. Therefore, the modern ephemerides is a means to track the state of all planets in the solar system at any

time of interest.

Many different versions of planetary ephemeris models exist. However the model chosen for the work presented is model 432t [32]. This model uses Chebyshev coefficients calculated by NASA's Jet Propulsion Laboratory (JPL). A pre-existing MATLAB function named "planetaryEphemeris.m" is available with the Aerospace toolbox and accesses ephemerides information real-time. Note that the ephemeris model determines the state of a planet in ICRF coordinates. Additionally, the ephemeris model for a given body accounts for the real orbital orientation for that planet in inertial space. There is no need to assume circular or co-planar orbits for this research, as the synergetic flyby analysis present in Chapter 3 is carried out in three dimensions with ease. Often times, it can be useful to include inclination changes coupled with gravitational assists. Such an example is the Ulysses spacecraft that was operated by NASA and the European Space Agency (ESA), which used a flyby of Jupiter to perform a change in inclination to its orbit well out of the ecliptic plane.

The ephemeris function that comes with the Aerospace toolbox is only used once for each body in the solar system at an epoch (reference time). The reason being, the function comes with some considerable computation cost. Further, this problem is only amplified as many function calls are made to it. When using a heuristic optimization method like Particle Swarm Optimization, often it is common to need to evaluate a function like the ephemeris function thousands of times. Therefore, that function is only used at an epoch, which was always chosen to be the launch date for the mission. For all other times, the state of bodies in the solar system are found by an analytic method, known as Lagrange coefficients. The benefit of Lagrange coefficients for propagating the solar system is that it saves valuable computational time versus the MATLAB ephemeris function.

When the state of an orbiting object $(\vec{r_0}, \vec{v_0})$ is known at some epoch $t_0$, then Lagrange coefficients are used in order to determine the state of an orbiting object at a future time $t$ is given by:

$$\vec{r} = f\vec{r_0} + g\vec{v_0} \tag{2.37}$$

$$\vec{v} = \dot{f}\vec{r_0} + \dot{g}\vec{v_0} \tag{2.38}$$

where

$$f = 1 - \frac{\mu r}{h^2}\left(1 - \cos\Delta\theta\right) \tag{2.39}$$

$$g = \frac{r r_0}{h}\sin\Delta\theta \tag{2.40}$$

$$\dot{f} = \frac{\mu}{h}\frac{1-\cos\Delta\theta}{\sin\Delta\theta}\left[\frac{\mu r}{h^2}\left(1-\cos\Delta\theta\right) - \frac{1}{r_0} - \frac{1}{r}\right] \tag{2.41}$$

$$\dot{g} = 1 - \frac{\mu r_0}{h^2}\left(1 - \cos\Delta\theta\right) \tag{2.42}$$

$$\Delta\theta = \theta - \theta_0 \tag{2.43}$$

$$r_0 = \sqrt{\vec{r_0}\cdot\vec{r_0}} \tag{2.44}$$

$$v_0 = \sqrt{\vec{v_0}\cdot\vec{v_0}} \tag{2.45}$$

$$r = \frac{h^2}{\mu}\frac{1}{1 + \left(\frac{h^2}{\mu r_0} - 1\right)\cos\Delta\theta - \frac{h v_{r0}}{\mu}\sin\Delta\theta} \tag{2.46}$$

$$h = |\vec{r_0}\times\vec{v_0}| \tag{2.47}$$

$$v_{r0} = \frac{\vec{r_0}\cdot\vec{v_0}}{r_0} \tag{2.48}$$

The Lagrange coefficients are found by first determining the true anomaly at the initial epoch, $\theta_0$ from two-body relations for elliptical orbits such as Eq. (2.9). The true anomaly at the time of interest, $\theta$, is found by simply iterating on Kepler's equation for an elliptical orbit using a scheme such as Newton-Raphson iteration presented in Eqs. (2.10-2.14). A fundamental derivation for the method of Lagrange coefficients is given by Curtis [1].

# Chapter 3
# The Solution Method

## 3.1 Linked Conics Approach

The research presented here is applicable for preliminary mission design purposes. Often, idealized models such as linked conics are an acceptable simplification for the level of fidelity desired for preliminary mission design. Here, linked conics assumes that a spacecraft instantly reaches the periapse of a flyby planet at encounter in the heliocentric frame (SICF). Therefore, the main consequence of this assumption is that the time of flight within the sphere of influence at each planet encountered is neglected when determining the trajectory to the next destination in the mission.

Although this assumption may seem crude at first glance, it actually models the dynamics fairly well due to the fact that the majority of the time of flight between planets is spent in the heliocentric frame. In other words, the spheres of influence for planets are small compared to the heliocentric distances traveled during the missions considered. As justification for this claim, consider the data for the average semi-major axes ($a_{AVG}$) for all planets in the solar system, included in Table 3.1. The ratio of the sphere of influence for each planet compared to its average distance from the Sun gives an idea of how small the time spent in the sphere of influence is compared to the much larger time of flight between planets.

A related assumption that follows from this model is that the velocity and position vector of each flyby planet is held constant during each flyby in the SICF. Put simply, the planet's change in position and velocity with respect to the Sun is neglected during relatively short time that the spacecraft spends in the planetocentric frame (PRCF).

Additionally, the time to fly from an Earth-centered orbit to the edge of the Earth's sphere of influence is also neglected when timing the flyby encounters for the fidelity desired from this research. Similarly, at the arrival destination there is

Table 3.1: Comparison between spheres of influence ($r_{SOI}$) and orbital semi major axes ($a_{AVG}$) in the solar system (data taken from Appendix A of Curtis [1]).

| Planet | $r_{SOI}\,(km)$ | $a_{AVG}\,(km)$ | $r_{SOI}/a_{AVG}\,(\%)$ |
|---|---|---|---|
| Mercury | 112,000 | 57,910,000 | 0.193 |
| Venus | 616,000 | 108,200,000 | 0.569 |
| Earth | 925,000 | 149,600,000 | 0.618 |
| Mars | 577,000 | 227,900,000 | 0.253 |
| Jupiter | 48,200,000 | 778,600,000 | 6.191 |
| Saturn | 54,800,000 | 1,433,000,000 | 3.824 |
| Uranus | 51,800,000 | 2,872,000,000 | 1.804 |
| Neptune | 86,600,000 | 4,495,000,000 | 1.927 |

not a consideration for time it takes the spacecraft to travel from the entrance into the final destination's sphere of influence to a parking orbit at a specified radius. Therefore, launch and arrival delta-v considerations include only the values in the SICF, and no Earth departure orbit or arrival parking orbit are assumed for this analysis.

## 3.2 Lambert's Problem

The problem of determining a specific trajectory connecting two given position vectors in space under some prescribed time of flight is commonly known as Lambert's problem. Figure 3.1 illustrates the geometry that defines this problem.

Lambert's problem is a well studied, cornerstone problem in the field of astrodynamics. Many prominant solution methods exist for solving the problem [33–36]. Each method has its own set of advantages and disadvantages for different problems. One might choose a certain method for a certain orbit regime. For example many Earth-orbiting analyses can be handled without the need for a universal-variable formulation of Lambert's problem because most Earth-orbiting applications are exclusively ones pertaining to closed orbits. Similarly, interplanetary trajectories are almost exclusively elliptical with respect to the Sun because hyperbolic orbits with respect to the Sun are difficult to achieve in practice, with the notable exceptions of Voyager 1 and Voyager 2.

However, this thesis has focus on Voyager 1 and Voyager 2 for design verification, which necessitates a method for solving Lambert's problem that can fluently shift between elliptical and hyperbolic cases. Additionally, the nature of the optimization

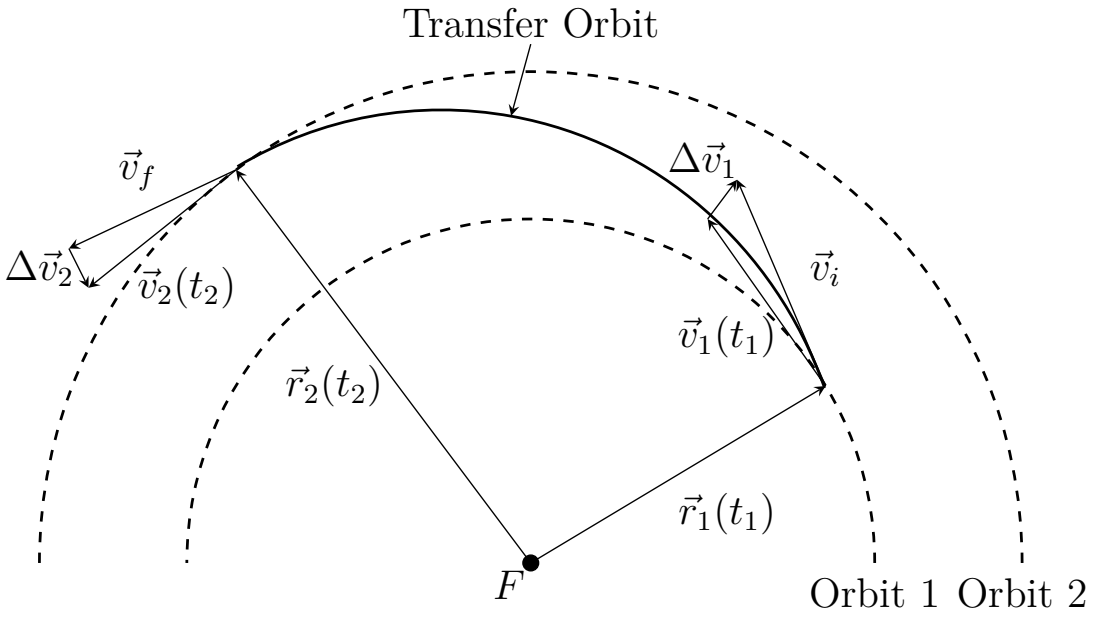


Figure 3.1: Lambert's problem geometry from inner orbit to outer orbit.

scheme for Particle Swarm Optimization for this MGA problem formulation involves random selection of flyby encounter dates.

The use of random processes to determine the dates gives some power to this optimization method, as it can search many options and trade-offs for flyby encounter dates that may not be intuitive. However, this strength comes with a noteworthy consequence. The dates chosen have no guarantee of producing elliptic orbits with respect to the Sun for transfers between planets. Careful consideration of this consequence dictates choosing a Lambert solution method that is robust under short times of flight. Although they will almost certainly require irrational amounts of propellant to execute, they inevitably end up being initial solutions considered by the optimization scheme, and must be planned for accordingly.

Here, the present research used Gooding's Method and utilized a MATLAB function created by the Johns Hopkins University's Applied Physics Laboratory [37]. The Lambert solution method has proven robust for all conic sections. This implementation of Gooding's method also includes capability to solve for trajectories between two points in space that make more than one revolution about the Sun. The ability to consider more than one revolution is most relevant to MGA missions involving inner planets. The method is well formulated with an iterative method known as the Halley method. The Halley method is similar to the well known Newton-Raphson method. However it achieves third-order convergence in the

Taylor series expansion used to solve for the universal parameter that defines the conic section for the solution. Most importantly, the method handles all conic sections well and calculates transfer trajectories in a timely and computationally efficient manner.

For the design of interplanetary trajectories that must involve MGA maneuvers, Lambert's problem must be solved from each planet to the next. From Earth launch to arrival at the desired destination, the number of times Lambert's problem is solved can be represented as a function of the number of flybys that will be executed:

$$N_{LP} = N_{FB} + 1 \tag{3.1}$$

The linked conics model for the flight from Earth to flyby planet(s) and from flyby planet(s) to destination planet dictates that the time of flight for any given transfer trajectory is found from the difference in the Julian dates at each respective planetary encounter as given by:

$$\begin{aligned} T_{total} = JD_A - JD_{FB_N} + JD_{FB_N} - JD_{FB_{N-1}} + ... + JD_{FB_2} - JD_{FB_1} \\ + JD_{FB_1} - JD_L = JD_A - JD_L \end{aligned} \tag{3.2}$$

where $T_{total}$ is the total time of flight for a MGA mission, $JD_L$ corresponds to the Julian date at launch, $JD_A$ corresponds to the Julian date at arrival, and each planetary flyby Julian date is denoted by its corresponding number such as $JD_{FB_N}$ corresponding to the $N^{th}$ flyby encounter and so on. The relationship of Eq. (3.2) could alternatively be framed as:

$$T_{total} = TOF_{NtoA} + TOF_{N-1toN} + ... + TOF_{1to2} + TOF_{Lto1} \tag{3.3}$$

where the notation for times of flight is such that $TOF_{NtoA}$ denotes the time of flight from flyby encounter $N$ to arrival and so on.

Again, the assumption of linked conics implies that the times of flight between bodies are from periapse in the initial planetocentric frame to periapse in the final planetocentric frame. Note also that Lambert's problem is solved identically from inner planets to outer planets as it is from outer planets to inner planets. For now, the missions that were considered for design verification were not ones requiring

multi-revolution consideration.

## 3.3 The Synergetic Flyby Problem

A synergetic gravity assist maneuver is one that couples a normal free-flight gravity assist trajectory with an impulsive engine burn by the orbiting spacecraft at the periapse of the flyby trajectory. The maneuver occurs in the flyby planet's local coordinate frame and can be thought of as having the same effect as the free-flight gravity assist maneuver, but with additional flexibility due to the ability to change the energy of the spacecraft's orbit with respect to the flyby planet.

There then exist two different hyperbolic orbits which the spacecraft has with respect to the flyby planet. The first is an incoming hyperbolic trajectory before the impulsive change in velocity occurs. The second is an outgoing hyperbolic trajectory after the impulsive change in velocity. The key advantage of a synergetic maneuver is the ability for the hyperbolic excess velocity to differ in magnitude between the incoming and the outgoing hyperbola so that, in general, it is assumed that:

$$v_\infty^- \neq v_\infty^+ \tag{3.4}$$

Normally with a free-flight gravity assist this difference in magnitude is not possible due to conservation of energy as the spacecraft encounters the flyby planet. However in this case, the spacecraft is changing the energy of its orbit with respect to the flyby planet. Additionally, there exist analytic limits on the scalar changes in velocity (as viewed in the Sun's coordinate frame) that can occur from a flyby for each planet in the solar system when considering only the free-flight gravity assist. A collection of these values appears in Table 3.2 as taken from Labunsky, Papkov, and Sukhanov [2] where a derivation using basic calculus can prove free-flight gravity assist maneuvers do abide by "speed limits" in effect.

These physical limits are critical to the formulation of the MGA problem in a normal case without consideration for synergetic capabilities. However, a synergetic gravity assist does not have these same theoretical upper bounds. In fact, the ability to consider maneuvers in conjunction with a flyby allows for additional solutions to potentially become feasible. The hyperbolic excess velocity with respect to the flyby planet can now change in both direction and magnitude. The formulation for the MGA problem in this thesis requires the ability to alter the

Table 3.2: Maximum scalar heliocentric velocity gain for free-flight gravity assists [2].

| Planet | $\Delta V_{max}\,(km/s)$ |
|---|---|
| Mercury | 3.01 |
| Venus | 7.33 |
| Earth | 7.91 |
| Mars | 3.55 |
| Jupiter | 42.73 |
| Saturn | 25.62 |
| Uranus | 15.18 |
| Neptune | 16.75 |

magnitude of the hyperbolic excess velocity with respect to the flyby planet. This requirement appears because the optimization algorithm is constructed so as to freely choose encounter times for flybys with planets. The times chosen may or may not coincide with a free-flight gravity assist. If every gravity assist maneuver was considered as a synergetic maneuver in general though, the method is more robust and allows more encounter times to be considered for solution. Just as with any spacecraft maneuver, the propellant consumption in terms of delta-v will be the factor determining whether a synergetic maneuver is practical or not. A spacecraft can gain more change in its post flyby heliocentric velocity if an impulsive maneuver also occurs. Figure 3.2 summarizes the flyby geometry, where the impulsive maneuver occurs specifically at periapse.

The manuever is idealized as impulsive, therefore the conventional two-body relations for a general hyperbolic orbit are valid for both the incoming and outgoing directions. Before and after the impulsive maneuver occurs, two-body relationships describe the incoming and outgoing hyperbolic trajectories:

$$\epsilon^- = \frac{v_\infty^{-2}}{2}\ ,\ \epsilon^+ = \frac{v_\infty^{+2}}{2} \tag{3.5}$$

$$a^- = -\frac{\mu_{FB}}{2\epsilon^-}\ ,\ a^+ = -\frac{\mu_{FB}}{2\epsilon^+} \tag{3.6}$$

$$e^- = \sqrt{\left(\frac{\Delta^-}{a^-}\right)^2 + 1}\ ,\ e^+ = \sqrt{\left(\frac{\Delta^+}{a^-}\right)^2 + 1} \tag{3.7}$$

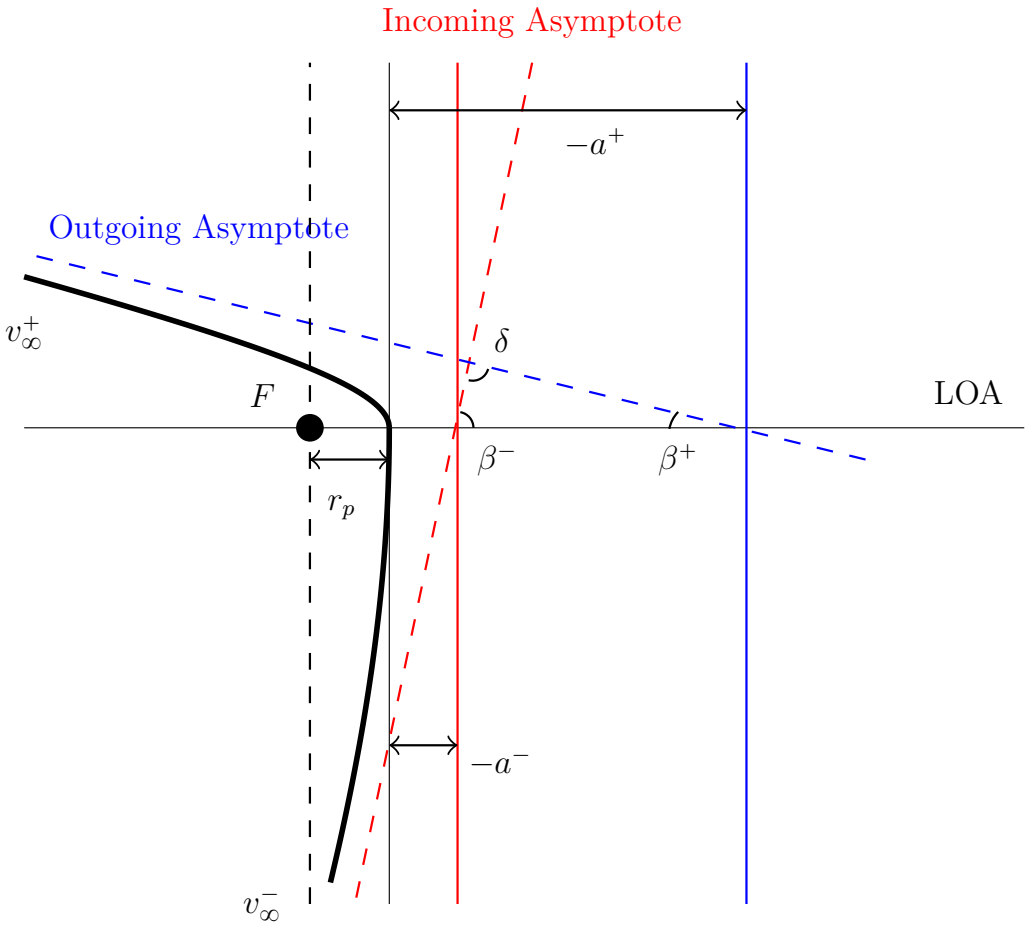


Figure 3.2: Synergetic flyby geometry.

$$\beta^- = \arccos\left(\frac{1}{e^-}\right) \ , \ \beta^+ = \arccos\left(\frac{1}{e^+}\right) \tag{3.8}$$

$$r_p^- = a^-\left(1 - e^-\right) \ , \ r_p^+ = a^+\left(1 - e^+\right) \tag{3.9}$$

$$v_p^- = \sqrt{2\left(\epsilon^- + \frac{\mu_{FB}}{r_p^-}\right)} \ , \ v_p^+ = \sqrt{2\left(\epsilon^+ + \frac{\mu_{FB}}{r_p^+}\right)} \tag{3.10}$$

$$\tan\beta^- = -\frac{\Delta^-}{a^-} \ , \ \tan\beta^+ = -\frac{\Delta^+}{a^+} \tag{3.11}$$

where $a < 0$ for a hyperbola, and the incoming trajectory is denoted by the superscript "-", whereas the outgoing trajectory is denoted by the superscript "+".

Additionally, this system of equations can be simplified in the case where the

incoming hyperbolic excess velocity vector and the outgoing hyperbolic excess velocity vector are both known. Due to the formulation of the MGA problem presented here, the vector quantities for hyperbolic excess velocities entering and leaving the flyby encounter are already determined from the solutions to Lambert's problem. With these in hand, their scalar magnitudes are easily found. Since a burn is to be applied at the periapse location (a location that is shared between both the incoming and outgoing hyperbolas), there is one unique impulsive manuever that satisfies the flyby encounter mathematically. The periapse burn is colinear with the two periapse velocity vectors on both the incoming and outgoing hyperbolic trajectories, and simplifies the value for the velocity change at periapse to:

$$v_p^+ = v_p^- + \Delta v_s \tag{3.12}$$

This means that the change in velocity will not change the line of apsides. An impulsive maneuver also means that the radius of periapse will not shift as a result of the engine burn. Immediately, Eq. (3.9) can be written as a consequence of this physical interpretation. This simplifies our system by introducing one new relationship between the incoming and outgoing hyperbolic orbits:

$$r_p = a^- \left(1 - e^-\right) = a^+ \left(1 - e^+\right) \tag{3.13}$$

There are simplifications that can be made to Eq. (4.7) from using the two-body relations developed in Eqs. (3.5-3.11). Thus, the periapse constraint can be rewritten in terms of the known hyperbolic excess velocity magnitudes, and the unknown eccentricities for each hyperbola:

$$\frac{v_\infty^+}{v_\infty^-} = \sqrt{\frac{1 - e^+}{1 - e^-}} \tag{3.14}$$

Although not entirely obvious, there are only two unknowns in this case: the eccentricities of the two separate hyperbolas. The first equation relating these two unknowns was established by Eq. (3.14). The second equation required to solve the system comes from the agreement between the geometry for the flyby (hyperbola shapes) and the physics of the orbital mechanics (velocity magnitudes). In this case, the hyperbolic excess velocity vectors into and out of the flyby were assumed as known. Therefore, the turn angle from the synergetic flyby can be obtained directly from the dot product between these two vectors.

$$\delta^* = \arccos\left[\frac{\vec{v}_\infty^- \cdot \vec{v}_\infty^+}{v_\infty^- v_\infty^+}\right] \tag{3.15}$$

The geometric turn angle must be satisfied by the incoming and outgoing hyperbolas, as shown by the triangle shown in Fig 3.2.

$$\delta = \pi - \left(\beta^- + \beta^+\right) \tag{3.16}$$

If the flyby is to be physical, then the two different formulations for the turn angles must agree:

$$\delta^* = \delta \tag{3.17}$$

It is possible to further simplify Eq. (3.17) in terms of the given hyperbolic excess velocities and the unknown eccentricities:

$$\arccos\left[\frac{\vec{v}_\infty^- \cdot \vec{v}_\infty^+}{v_\infty^- v_\infty^+}\right] = \pi + \arctan\sqrt{(e^-)^2 - 1} + \arctan\sqrt{(e^+)^2 - 1} \tag{3.18}$$

At this point, there are now two equations, and two unknowns. Eqs. (3.14) and (3.18) can be solved for $e^-$ and $e^+$ by any method that handles a system of two nonlinear algebraic equations.

A successful method chosen for the present research is a multivariate Newton-Raphson scheme that iterates on the unknown variables of the system until a convergence criterion is reached. Here, the vector of the unknowns $e^-$ and $e^+$ is constructed for the $i^{th}$ iteration as:

$$\mathbf{X}_i = \begin{bmatrix} e^- \\ e^+ \end{bmatrix}_i \tag{3.19}$$

The system of two nonlinear algebraic equations can then be written in the form:

$$\mathbf{F}(e^-, e^+) = \begin{bmatrix} f_1 \\ f_2 \end{bmatrix} = \begin{bmatrix} 0 \\ 0 \end{bmatrix} \tag{3.20}$$

where

$$\begin{bmatrix} f_1 \\ f_2 \end{bmatrix} = \begin{bmatrix} \pi - \arccos\left[\frac{\vec{v}_\infty^- \cdot \vec{v}_\infty^+}{v_\infty^- v_\infty^+}\right] + \arctan\sqrt{\left(e^-\right)^2 - 1} + \arctan\sqrt{\left(e^+\right)^2 - 1} \\ v_\infty^{-2}\left(1 - e^+\right) - v_\infty^{+2}\left(1 - e^-\right) \end{bmatrix} \tag{3.21}$$

The Jacobian for the system of equations is then:

$$\mathbf{J}(e^-, e^+) = \begin{bmatrix} \frac{\partial f_1}{\partial e^-} & \frac{\partial f_1}{\partial e^+} \\ \frac{\partial f_2}{\partial e^-} & \frac{\partial f_2}{\partial e^+} \end{bmatrix} = \begin{bmatrix} \frac{1}{e^-\sqrt{(e^-)^2-1}} & \frac{1}{e^+\sqrt{(e^+)^2-1}} \\ \left(v_\infty^+\right)^2 & -\left(v_\infty^-\right)^2 \end{bmatrix} \tag{3.22}$$

The correction to the vector of unknowns is found at each iteration via the relationship for a first-order Taylor series expansion as:

$$\delta\mathbf{X}_i = -\mathbf{J}^{-1}(\mathbf{X}_i)\,\mathbf{F}(\mathbf{X}_i) \tag{3.23}$$

The iterations are carried out over index $i$ such that convergence is reached when:

$$\mathrm{RMS}\left(\delta\mathbf{X}_i\right) \leqslant \Delta_A \tag{3.24}$$

where RMS is the root mean square operation and $\Delta_A$ is a user-specified tolerance. For this research, the absolute tolerance of $\Delta_A = 1 \times 10^{-10}$ was used. If convergence is not reached, then the vector of unknowns is updated by:

$$\mathbf{X}_{i+1} = \mathbf{X}_i + \delta\mathbf{X}_i \tag{3.25}$$

A favorable initial guess for such a system was determined to be a nearly parabolic orbit, offset by the absolute tolerance value:

$$\mathbf{X}_0 = \begin{bmatrix} 1 + \Delta_A \\ 1 + \Delta_A \end{bmatrix} \tag{3.26}$$

This choice of the initial guess guaranteed well-behaved iterative updates to $e^-$ and $e^+$, such that mathematical singularities in the Jacobian of Eq. (3.22) are avoided for the case where $e^-$ or $e^+$ take value of 1. The final values of $e^-$ and $e^+$ obtained from the iterative scheme can then be used to determine the other parameters of the system. The parameters of interest for evaluating the feasibility of a synergetic

flyby maneuver are radius of periapse and the magnitude of the synergetic delta-v. Both are calculated by substituting the newly found eccentricities into the system shown in Eqs. (3.5-3.11).

It is important to note that there is a single unique set of unknown eccentricities that satisfies the solution to the system of equations given by $\mathbf{F}$ for any flyby with known velocity vectors into and out of the sphere of influence.

# Chapter 4
# Particle Swarm Optimization

## 4.1 General Background

Particle Swarm Optimization (PSO) is a non-rigorous, heuristic algorithm that is based on the natural phenomenon of a swarm of insects, birds, or fish as they hunt for prey. PSO is one formulation in a category of algorithms that solve optimization problems by heuristic means. Other comparable algorithms include differential evolution (DE), firework optimization, or bacteria foraging optimization. These algorithms all share the commonality that their structure and philosophy stem from observation and depiction of some kind of natural or physical phenomenon. The PSO algorithm is useful for multi-variable optimization problems in particular, where trade-offs between decision variables of a problem are to be explored for identification of potential optimal solutions. Heuristic optimization methods like PSO do not guarantee global optimal solutions, nor in general is there an analytic proof that a solution found from a heuristic method is the globally optimal solution. However, these methods do provide as good a chance as any other method in cases where a problem does not lend itself to a formulation that allows for use of the more mathematically rigorous gradient-based methods. In this way we come to the major reason that these types of methods are attractive to solving complex problems. One of the large benefits to using a method such as PSO is the potential that it holds for searching large solution spaces with reasonable computational expense.

Potential solutions are formally quantified and evaluated for their "goodness" by means of a cost function. The cost function is a mathematical representation of some desired outcome or preferred condition for a problem's solution. The optimization problem is formulated as that of a minimization problem involving the cost function. The amount of time that it takes for an algorithm like PSO to produce

a solution to an optimization problem largely depends on the amount of time it takes to do necessary computations to evaluate the cost function (often referred to collectively as the function evaluation). The function evaluations are problem specific, and often are computationally expensive for complex problems. Often in the cases where computational efficiency is lacking for the function evaluation of a problem, there is not an analytic modeling technique present. A common reason to turning towards using a heuristic optimization method in the first place is because a problem may not be feasible to solve with any other known method. In this way, the heuristic optimization method is at least a way of tackling complex problems that may go otherwise unsolved.

Along the way to evaluating an optimal solution, PSO does not formally enforce equality constraints. Due to this fact, formulations of cost functions will often incorporate the use of weights to provide preference towards certain aspects or components of the overall cost function. For example, the weights are often used to scale and emphasize undesirable component(s) of the cost function, such as penalty terms. Applying large weights to penalty terms can prove very effective for weeding out undesired outcomes from a solution, however there is no guarantee that the solutions produced will always satisfy a desired condition. This reality is something that must be understood prior to applying this method to engineering problems. Often times, solutions obtained may provide a valuable insight (even with violated equality constraints) compared to no solution at all.

## 4.2 Algorithm Structure

As previously mentioned, PSO has been around since the mid 1990's. As the years have passed, researchers have encountered a stagnation effect where the algorithm settles upon local minima for certain problems, instead of fully investigating the search space [26]. As a result, new variants on the optimization method have been created, which alter the traditional behavior of the classic PSO algorithm. However, for the application of this thesis a classic algorithm formulation first introduced by Eberhart and Kennedy [19] proves satisfactory when solving this formulation of the MGA optimization problem.

The classic PSO algorithm is centered around the concept of a swarm of particles that are "flying" or moving through the solution space for the user defined problem. The solution space is the mathematical space defined by the domain of all of the

possible values of each decision variable ($N_{variables}$) that a user wishes to optimize over. A particle represents a unique set of chosen variable values that form a completely defined solution to the optimization problem. The particle's placement in the solution space is termed the "position" (denoted $\mathbf{p}_j$), and simply corresponds to the unique spot in the solution space corresponding to all of the specific values for the decision variables in that particle. Each particle has its own associated cost as its components (decision variable values) pass through a cost function. A user specified number of particles ($N_{particles}$) make up what is known as the swarm. The more particles that make up a swarm, the more breadth the swarm has to examine the solution space. The user must be weary of using too many particles though, as this increases computational time as more particles lead to more calculations per iteration. A general rule of thumb for the method has become ten times the number of variables that the user wishes to optimize for. To start the algorithm, the "positions" of all particles are uniformly randomized. However, before a user can apply PSO to a problem, a general idea of what domain the solution space should cover is required. The general knowledge of what range the decision variables can take is applied directly inside of the algorithm through upper and lower bounds ($\mathbf{b}_{lower}, \mathbf{b}_{upper}$). The upper and lower bounds for decision variables define the space within which particles can move.

The general methodology allows these particles to move through the solution space with a "velocity" (denoted $\mathbf{v}_j$), which is the rate at which a particle's "position" changes per iteration. The rate of change is determined by three main components. Each "velocity" component has a randomized weight determining its contribution to the total velocity. The first contribution is the inertial component of the "velocity" (with weight $c_I$), which keeps a given particle moving in the direction that its motion in the solution space has already been directed along (analogous in thought to a Newtonian inertia for a ball or small mass). The second contribution comes from a cognitive ability that each particle possesses. This cognitive ability comes from the particle knowing and remembering where its own best solution has been found in the solution space (with weight $c_C$). The last component to the velocity comes from a social aspect of the particles. Each particle is a part of the population that makes up the swarm. With that role, the particle also has a component of its velocity that drives it toward the global best solution ever seen by the entire swarm (with weight $c_S$). If a particle should gain enough "velocity" to exceed outside of the bounds (either upper or lower) for the solution space as specified by the user,

then the particle is placed at a "position" at the boundary with a "velocity" of zero.

The motion of the particle in the solution space is carried out over a finite number of iterations specified by the user ($N_{iterations}$). More iterations will allow the particles to proceed in motion through the solution space for longer, which potentially means a deeper, more exhaustive search of the solution space. Again, the user should be weary of executing too many iterations though, as this slows down the computation time. Commonly, the notion of convergence for the algorithm is useful for deciding how many iterations are sufficient for a given problem. The algorithm is typically ran for a short number of iterations at first, and the convergence of the algorithm in terms of a cost function is monitored by tracking the best value for that cost function that the swarm has ever encountered (defined as $J_{Best,G}$). A logarithmic behavior for $J_{Best,G}$ over the number of iterations is preferable, and shows that the algorithm has most likely settled within the solution space on a minima. As previously mentioned, there is no guarantee that this minima is global in nature. Sometimes certain problems can cause the algorithm to stagnate for a given run, as the swarm settles in a local minima. This behavior requires re-initializing the entire algorithm and running it again in the hopes of avoiding that outcome in the future. After the motion of the particles is carried out for all iterations, the global best "position" of a particle ever achieved is viewed as the optimal solution to the multi-variable optimization problem. The general methodology for PSO is summarized in Algorithm 1.

**Algorithm 1** Particle Swarm Optimization Algorithm, based on the Eberhart and Kennedy formulation [19]

**procedure** PSO($N_{iterations}, N_{particles}, \mathbf{b}_{lower}, \mathbf{b}_{upper}$)
  **for** $i = 1 : N_{iterations}$ **do**
    **for** $j = 1 : N_{particles}$ **do**
      $J_j = \text{cost}(\mathbf{p}_j)$
      **if** $J_j < J_{Best,j}$ **then**
        $J_{Best,j} = J_j$
        $\mathbf{p}_{Best,j} = \mathbf{p}_j$
      **if** $J_j < J_{Best,G}$ **then**
        $J_{Best,G} = J_j$
        $\mathbf{p}_{Best,G} = \mathbf{p}_j$
      $c_I = \frac{1+r_1(0,1)}{2}$ , $c_C = 1.49445\, r_2(0,1)$ , $c_S = 1.49445\, r_3(0,1)$
      $\mathbf{v}_j^* = c_I\, \mathbf{v}_j + c_C\, (\mathbf{p}_{Best,j}$ - $\mathbf{p}_j) + c_S\, (\mathbf{p}_{Best,G}$ - $\mathbf{p}_j)$
      $\mathbf{p}_j^* = \mathbf{p}_j + \mathbf{v}_j$
      **if** $\mathbf{p}_j^* > \mathbf{b}_{upper}$ **then**
        $\mathbf{p}_j^* = \mathbf{b}_{upper}$
        $\mathbf{v}_j^* = \mathbf{0}$
      **else if** $\mathbf{p}_j^* < \mathbf{b}_{lower}$ **then**
        $\mathbf{p}_j^* = \mathbf{b}_{lower}$
        $\mathbf{v}_j^* = \mathbf{0}$
      $\mathbf{p}_j = \mathbf{p}_j^*$
      $\mathbf{v}_j = \mathbf{v}_j^*$
      **return** $\mathbf{p}_{Best,G}$

Additionally, a two-dimensional visualization of the algorithm's process of updating a particle's position and velocity is provided in Figure 4.1.

## 4.3 The Multiple Gravity Assist (MGA) Problem Formulation

PSO is based on the principle that each particle of the swarm holds a fully-defined solution to the optimization problem at hand. For this thesis, the goal is to optimize the flyby dates for missions with a prescribed planetary sequence, meaning that the number of planets and the order that they occur is already predetermined. Additionally, the launch and arrival dates for the mission are assumed as known.

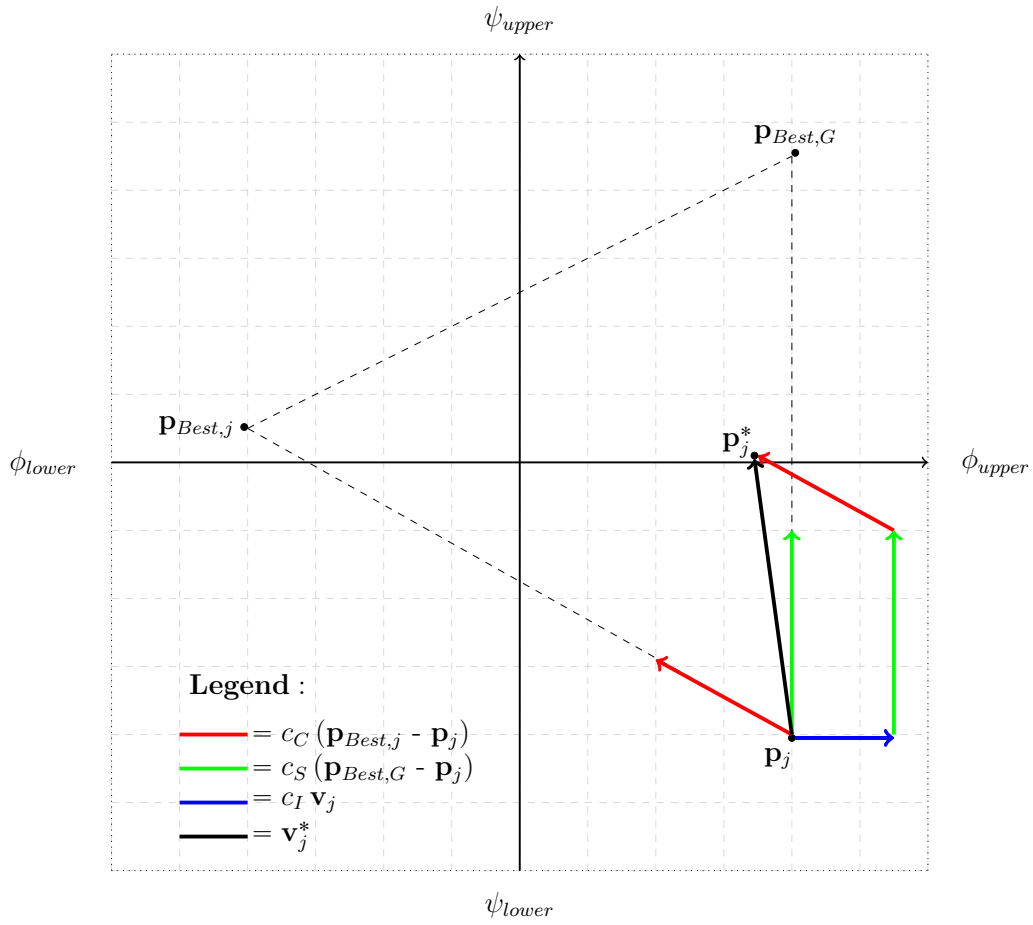


Figure 4.1: A visual representation of the process for updating "position" and "velocity" of a $j^{th}$ particle in PSO. Here, there are two decision variables $\phi$ and $\psi$.

Therefore, an individual particle for this MGA optimization problem consists of a vector containing each Julian date for the $N_{FB}$ flybys necessary to execute a certain desired mission.

$$\mathbf{p}_j = [JD_{FB_1}, ..., JD_{FB_N}] \tag{4.1}$$

A practical set of bounds can be any date between the specified launch date and the specified arrival date. In practice, it is found that solutions converge more effectively when a small buffer time is introduced such that the available flyby dates of choice fall within upper and lower bounds of:

$$\mathbf{b}_{lower} = [JD_L + 10, ..., JD_L + 10\,N_{FB}] \tag{4.2}$$

$$\mathbf{b}_{upper} = [JD_A - 10, ..., JD_L - 10\,N_{FB}] \tag{4.3}$$

This buffer time helps to avoid the physically impossible Lambert trajectories for near zero times of flight. A 10 day buffer on either side of dates proves to be sufficient enough to avoid the singularity, without constricting the solution space in a significant way.

The algorithm evaluates a cost function using each particle's flyby dates for a series of prescribed iterations. For a given iteration, the global best particle (or solution) and the best solution found for each particle are saved. All other particles are influenced by these solutions for the next iteration. A particle "velocity" is influenced by means of inertial, cognitive, and social acceleration coefficients, where $r_1(0,1), r_2(0,1)$, and $r_3(0,1)$ are three different random numbers found using a uniform distribution from 0 to 1. A version of the classic PSO is used that incorporates acceleration coefficients as:

$$c_I = \frac{1 + r_1(0,1)}{2}\ ,\ c_C = 1.49445\, r_2(0,1)\ ,\ c_S = 1.49445\, r_3(0,1) \tag{4.4}$$

from well-established spaceflight trajectory optimization research [22]. These acceleration coefficients randomly influence the motion all of potential solutions across all particles and all iterations.

For a given iteration of the PSO algorithm, the set of flyby dates from each particle in the population is used to determine the Lambert's solution trajectory (or trajectories for multiple flybys) corresponding to that particle. Whether or not that flyby is physically possible is then handled by a calculation for the synergetic maneuver required to support the heliocentric change in velocity necessary to connect any two adjacent Lambert's solution trajectories. Evaluation of the synergetic maneuvers involves examining the periapse radii and the synergetic delta-v required to execute a certain flyby circumstance. In essence, every flyby that is necessary can be viewed as a synergetic maneuver. The free-flight gravity assist (that requires no propellant to be expended by a spacecraft) is recovered as a simplification of the synergetic flyby.

The cost function that is used to evaluate the feasibility of a given mission schedule is a combination of propellant expenditures, as well as the closest approach that the spacecraft makes with respect to the flyby planet. The cost function has a delta-v associated with departure from Earth (SICF), a delta-v associated with

arrival at the destination location (SICF), and $N_{FB}$ number synergetic delta-v manuevers (PRCF):

$$J = |\Delta\vec{V}_L| + |\Delta\vec{v}_{s_1}| + ... + |\Delta\vec{v}_{s_N}| + |\Delta\vec{V}_A| + w_p|\min[0, r_p - r_{p,min}]| \tag{4.5}$$

or

$$J = \Delta V_L + \Delta v_{s_1} + ... + \Delta v_{s_N} + \Delta V_A + w_p|\min[0, r_p - r_{p,min}]| \tag{4.6}$$

with a minimum periapse radius defined as:

$$r_{p,min} = R_{FB} + h_{p,min} \tag{4.7}$$

where the minimum acceptable altitude at periapse is $h_{p,min}$, the flyby planet's radius is $R_{FB}$, and the weight value associated with the periapse penalty term is $w_p$..

The close approach distance (radius of periapse) with respect to a flyby planet only affects the evaluation of the cost function if the distance is to end up inside of the minimum desired radius of periapse. This penalty is created to serve as a periapse violation penalty. There is no penalty term contributing to the cost function evaluation for a given solution as long as its radius of periapse is larger than the minimum desired radius of periapse. The minimum acceptable altitude at periapse is $h_{p,min} = 500$ kilometers. In the event that a trajectory requires the penalty term, the weight value must be positive and measured in units of $(1/s)$. For this research, the value of the weight is assigned as $w_p = 1.00\,(1/s)$ such that the value of the violation distance (in kilometers) is added to the cost function. This weight value proves plenty effective for the cases presented in this thesis, because the magnitude of the distance is often many orders of magnitude larger than the order of magnitude of the delta-v terms. This difference in order of magnitude applies a useful and large enough penalty to deter particles away from solutions that violate the desired periapse constraint. If a penalty of a much larger value approaching infinity is chosen, then it becomes more likely that the swarm can diverge away from some trajectories that might be relatively low in altitude, but feasible in all other respects.

The determination of the number of iterations was carried out by trial and observation for small numbers of iterations, on the order of 10 to start. Logarithmic

convergence was desired, and as a result the iteration number was increased to achieve that effect. After trial and observation, a desired number of iterations for this problem is found to be 100. Additionally, it is often the case that a heuristic method should be attempted over multiple trials before a common result is obtained and validated. For this problem in particular, the optimal solution reappears for 7 or more times out of a set of 10 trials.

# Chapter 5
# Results and Findings

## 5.1 Verification for a New Method

The focus of this thesis is to develop a new method to design trajectories for missions with known planetary sequences and desired launch and arrival times. However, it is necessary to first prove that the methodology developed compares well with solutions that already exist or that have already been solved in an effective way. In the past, there have been some very successful missions that have leveraged the use of more than one gravitational assist. These missions have flown to distant targets that may have otherwise been impossible to visit or have been designed with more than one gravity assist in order to substitute large amounts of propellant for larger payloads that may otherwise prove unfeasible. Three well known examples of missions that have utilized more than one gravity assist are Voyager 1, Voyager 2, and Cassini. It cannot be known for sure whether or not these trajectories are optimal in the global sense, however there is reasonable intuition that points to Voyager 1 and Voyager 2 as being near optimal trajectories for the mission that they were designed to accomplish. The goal of the set of missions was to flyby the outer gas giants, and pass by as many of them as possible with the hopes of eventually gaining enough energy to escape the solar system entirely. These missions are still in motion on the other side of the heliopause as of today, and successfully demonstrated the significance that sequencing more than one gravity assist holds for the process of mission design. There exists no analytic way to prove that Voyager 1, Voyager 2, or Cassini were globally optimal solutions to their mission design problems. In general, this is not something available for a mission designer to rely upon. There exists no simple analytic formulation for the MGA problem. This reality makes it difficult to prove or verify a new method when it is applied to this MGA problem. For this reason, the best comparison that exists is

to look back at past missions in order to compare results from the new method using PSO to what has previously flown. If results from PSO are similar to those seen in these previous missions, then one can conclude that the method for design has the chance to be viewed as credible when application is then turned to new mission design problems. In addition to precursor missions, there is consideration for a new mission design case in this chapter.

Before applying any optimization techniques, the before mentioned missions are modeled with the dynamics and assumptions established earlier in this thesis. In addition to involving multiple gravity assist maneuvers, these missions specifically utilize free-flight gravity assist maneuvers. Although the synergetic flyby is the model for flybys examined in thesis, these missions also provide an opportunity for verifying the synergetic flyby analysis developed as part of this thesis. For trajectories that involve free-flight gravity assist maneuvers, the synergetic flyby analysis simplifies to the free-flight case. This fact emerges as part of the model trajectories for Voyager 1, Voyager 2, and Cassini. In addition, there exists data open to the public through NASA's Planetary Data System (PDS) [38] covering key milestones for all of these missions in some capacity. The model is comparable against the flyby altitude data from NASA's PDS, providing a reasonable level of verification for the solution method presented in this thesis.

In order to examine Voyager 1 and Voyager 2 side by side against a PSO solution, the missions are viewed in a way similar to the MGA problem with a definite launch location and arrival destination. Here, the two spacecraft in fact have no ending destination for their missions. However, truncating the last flyby of the two missions and instead viewing those planets as the arrival destinations creates a comparable formulation to the MGA problem outlined previously in this thesis. An important note is that all real missions include trajectory correction manuevers that ever so slightly correct the course for a trajectory. This is necessary, as real trajectories are subject to realistic effects that are not always captured in modeling (especially preliminary, low fidelity modeling). Similarly, when comparing a PSO solution to the Cassini mission trajectory, it is important to note that the real mission involved a non-negligible targeting maneuver that is not modeled with the MGA problem formulation. However, this mission case still proves to be yet another trajectory that is closest in nature to the MGA problem formulated here. In fact, examination of the Cassini mission allows for an opportunity to compare the choice of a deep-space targeting manuever versus a maneuver executed in conjunction

with a flyby. Another beneficial outcome from choosing these missions is that they offer the chance to incrementally introduce more and more decision variables (flyby dates) to the optimizer. This way, the optimizer's performance is observed as the solution space grows in dimension.

For the results comparisons made in this section, each mission is modeled with the real dates of launch, flyby encounters, and destination arrivals. The results serve as the direct comparison case against any PSO mission trajectory produced, because they have the same level of fidelity in terms of dynamic model. However, real mission data for things like flyby altitudes was taken from NASA and included for reference wherever possible. There is not an expectation that every piece of real mission data gathered will match perfectly with all modeled values, because there is a significant difference in the level of fidelity between the model and a real-life scenario. Therefore, the real mission values are included in an effort to provide some context as to how closely each modeled trajectory come to the ground truth, not necessarily in an effort to do any serious analysis of error between the model and the ground truth. Additionally, it is not fair to conclude that any PSO mission trajectory is superior in nature to that which flew in real-life, because there are many driving factors to mission design that are not accounted for in the preliminary model. As one example, launch dates often slip due to unforeseen circumstances for space missions. These type of events have an effect on the real trajectories and their cost in regards to propellant, flyby altitudes, and so on. However, preliminary mission design trajectories are proposed in an idealized situation where those things are not directly affecting the analysis.

## 5.2 Optimized Results

The results presented in this thesis are ones obtained by execution of program files written in MATLAB 2017a on a 3.06 GHz Intel Core 2 Duo 2009 iMac. In all results presented, the planets are indicated by various colored orbits. Tables 5.1-5.2 summarizes the legend for identifying the planets, as well as the coloring of trajectories for all mission cases to be examined. Results from the computations are shown in Tables 5.3-5.6 for each of the cases examined. The results of interest from analysis are flyby dates, scalar synergetic delta-v values required at each flyby encounter, radii (or altitudes) of peripase, scalar heliocentric delta-v values at launch, flybys, and arrival planets, and cost function associated with each

mission solution. Note that the heliocentric delta-v value for flyby encounters is not a contributing part of the cost function. However, its numerical value remains useful for purposes of comparison against values shown previously in Table 3.2 to demonstrate the increased flexibility that synergetic gravity assist maneuvers provide mission designers.

Table 5.1: A color legend for the orbits of the planets.

| Planet | Color |
|---|---|
| Mercury | Brown |
| Venus | Violet |
| Earth | Dark Green |
| Mars | Dark Red |
| Jupiter | Orange |
| Saturn | Yellow |
| Uranus | Cyan |
| Neptune | Blue |

Table 5.2: A color legend for the plotted mission trajectories.

| Trajectory | Color |
|---|---|
| Voyager 1 | Bright Green |
| Voyager 2 | Bright Blue |
| Cassini | Dark Bright Red |
| PSO Result | Black |
| PSO Designed, 3 year | Solid Pink |
| PSO Designed, 4 year | Solid Light Blue |
| Direct Designed, 3 year | Dashed Pink |
| Direct Designed, 4 year | Dashed Light Blue |

### 5.2.1 Voyager 1 Case

Voyager 1 is the first trajectory design case. Voyager 1 launched from Earth on September 5th, 1977. As mentioned previously, Voyager 1 is still to this day traveling through heliopause on its way outside of our solar system. The final destination as viewed in the MGA problem is chosen as that of Saturn, which is the last flyby encounter that Voyager 1 saw before heading towards the edge of the solar system. Voyager 1 reached Saturn on November 12th, 1980 on its real-life trajectory. The trajectory required one flyby at Jupiter between a launch from

Earth and an arrival at Saturn. The real flyby of Jupiter occurred on March 5th, 1979 with a closest approach radius from the center of Jupiter corresponding to 348,890 kilometers. This mission serves as a good starting point, since it only involves optimizing one decision variable for the MGA problem ($N_{FB} = 1$).

PSO is an algorithm that works most effectively to solve a problem when it is run more than one time. The first run of the algorithm often does not prove to be the best, and more reliable solutions are found when PSO is ran for a series of trials and the best solution is chosen from the group of trials. The best result of this mission design was found after running 10 trials of PSO and is presented here. The solution takes 100 iterations, with a swarm population of 50 particles, and elapses 40.58 seconds of wall clock time. The algorithm shows signs of convergence as early as 20 iterations or so (see Figure 5.1). However, it is best to run the algorithm beyond this number of iterations to guarantee that no better solution are obtained.

PSO has free selection of a Julian date for the flyby encounter of Jupiter that range from 10 days after launch date, and 10 days before arrival date. The optimal flyby date as viewed by the optimizer is March 5th, 1979 with a closest approach radius from the center of Jupiter corresponding to 340,664 kilometers. For direct comparison, the actual dates for Voyager 1 are passed through the dynamic model, where the closest approach radius from the center of Jupiter corresponds to 341,099 kilometers. The flyby manuevers are expected to simplify from synergetic maneuvers of sizeable magnitude towards ones of very little change in velocity approaching a free-flight case. The results of Table 5.3 show that Voyager 1 can be modeled with synergetic flybys of very small magnitude changes in velocity at periapse. Additionally, it is clear that the solution as found by PSO is very similar in nature to that modeled using the real mission dates. No violations of the periapse radius for the flyby are present in either case. With that detail in mind, both the modeled mission and the PSO optimized mission return flybys that are feasible results from an engineering perspective.

Overall, the results for one decision variable using PSO on the MGA problem prove promising and give an indication that the methodology is successful in a preliminary design sense. PSO is even able to identify favorably performing solutions early on in most of the trials, with very few trials returning trajectories that had large variations from the Voyager 1 mission model. Figure 5.3 shows how similar the two solutions were, with the black PSO trajectory falling closely on top of the bright green mission model trajectory.

Table 5.3: Comparison of results between optimal case and Voyager 1 mission ($N_{FB} = 1$).

| Mission | Flyby | Date | $\Delta v_{s_N}\,(km/s)$ | $r_p\,(km)$ | $\Delta V_L\,(km/s)$ | $\Delta V_{FB}\,(km/s)$ | $\Delta V_A\,(km/s)$ | $J\,(km/s)$ |
|---|---|---|---|---|---|---|---|---|
| PSO | Jupiter | 03/04/1979 | $1.5739 \times 10^{-12}$ | $340,664$ | 10.2360 | 16.5837 | 15.2707 | 25.5067 |
| Voyager 1 | Jupiter | 03/05/1979 | 0.0171 | $341,099$<br>Real [38]: $348,890$ | 10.2275 | 16.5736 | 15.2866 | 25.5312 |

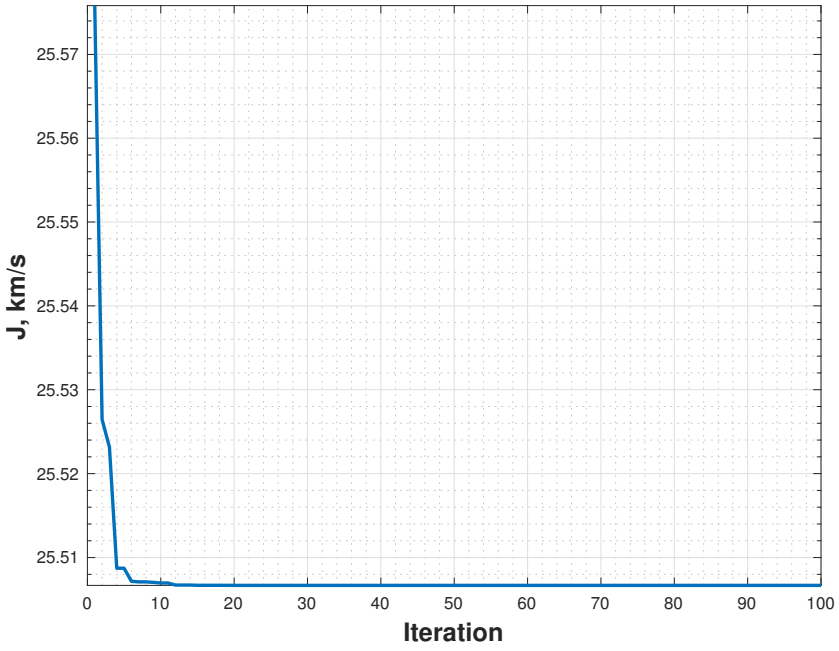


Figure 5.1: PSO cost function convergence vs. iteration number for Voyager 1 (log scale y-axis).

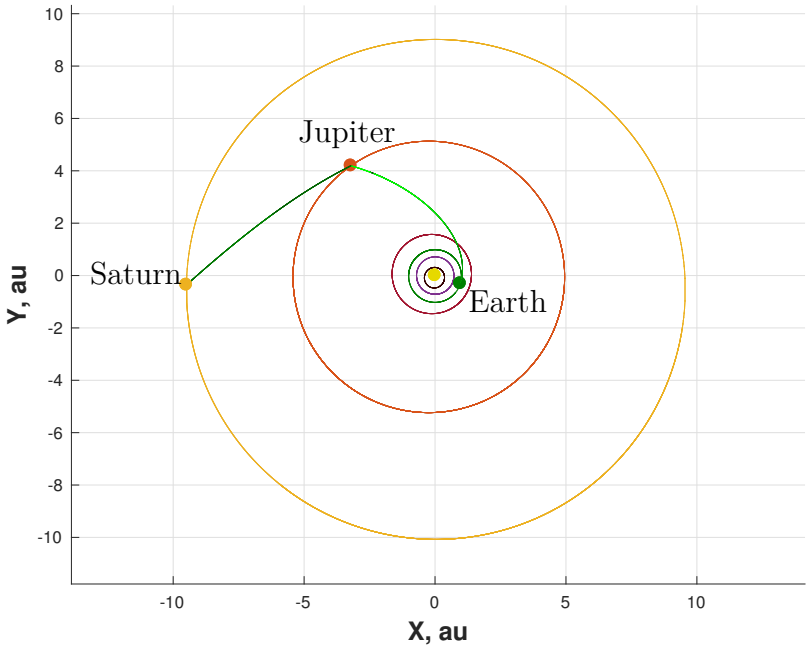


Figure 5.2: The optimal result from PSO vs. the actual Voyager 1 mission dates (SICF).

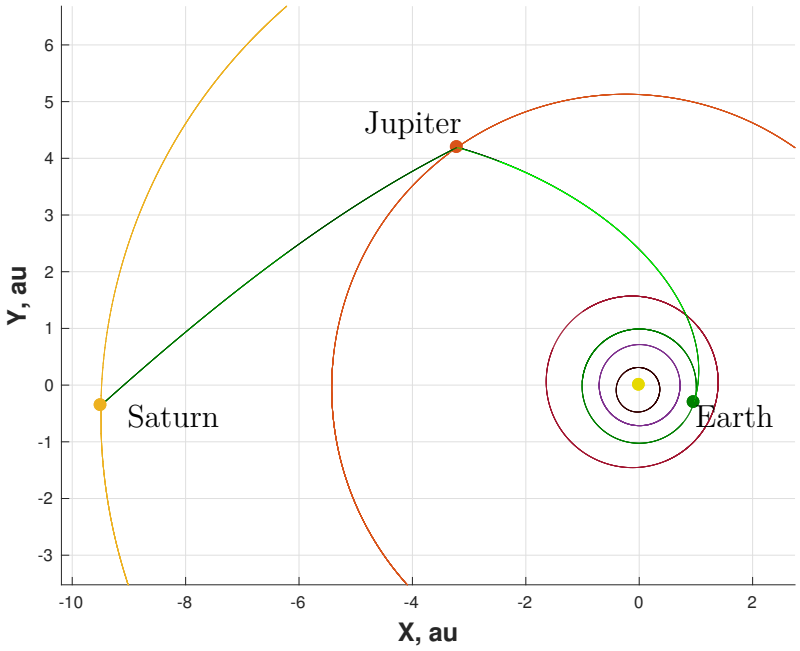


Figure 5.3: The optimal result from PSO vs. the actual Voyager 1 mission dates (closer view, SICF).

### 5.2.2 Voyager 2 Case

Voyager 2 is selected as the second trajectory design case and provides an increase in the number of decision variable for the MGA problem ($N_{FB} = 3$). Voyager 2 launched from Earth on August 20th, 1977. Voyager 2 is now also on a journey traveling outside of the solar system. The final destination chosen for this model is Neptune, which is the last flyby encounter that the spacecraft saw before heading towards the edge of the solar system. Voyager 2 reached Neptune on August 25th, 1989 in real-life. The trajectory reached Neptune by first encountering three planets for planetary flybys. The first flyby was that of Jupiter, on July 9th, 1979 at a closest approach radius of 721,670 kilometers from the planet's center. The second flyby was that of Saturn on August 26th, 1981 at a closest approach radius of 161,000 kilometers from the center of the planet. Finally, the last flyby was of Uranus on January 24th, 1986 with a closest approach radius of 107,000 kilometers from the center of the planet.

The best result of this mission design is found after running 10 trials of PSO. The solution takes 100 iterations, with a swarm population of 50 particles, and elapses

77.77 seconds of wall clock time. The algorithm has slightly slower convergence compared against that of the Voyager 1 mission, as shown in Figure 5.4, due to the increase in the number of decision variables that PSO has choice over.

PSO has free selection of the Julian dates for the three flyby encounters (Jupiter, Saturn, Uranus) from 10 days after launch date, 10 days before arrival date, and 10 days after or before any flyby (as the algorithm chooses the dates one at a time). The optimal flyby date for Jupiter as viewed by the optimizer is July 14th, 1979 with a closest approach radius from the center of Jupiter corresponding to 709,578 kilometers. The optimal flyby date for Saturn is chosen as August 31st, 1981 at a closest approach radius of 157,238 kilometers. The optimal flyby date for Uranus is selected to be January 25th, 1986 at a closest approach radius of 106,993 kilometers.

For direct comparison, the actual dates for Voyager 2 are passed through the dynamic model, where the closest approach radius from the center of Jupiter corresponded to 701,801 kilometers, Saturn corresponded to 341,099 kilometers, and Uranus corresponded to 107,039 kilometers. The flyby manuevers are again similar to those of very little change in velocity, approaching a free-flight case (like with Voyager 1). The results of Table 5.4 show that Voyager 2 can be modeled with synergetic flybys of very small magnitude changes in velocity at periapse, as anticipated. Additionally, it is again clear that the solution found by PSO is very similar in nature to that modeled using the real mission dates. Just as seen for the mission with Voyager 1, there are no violations of the periapse radius for the flyby in either case. It is clear that the modeled mission and the PSO optimized mission both return a set of flybys that are reasonable enough for preliminary design.

This mission shows that the results for three decision variables using PSO on the MGA problem are encouraging and give another indication that the methodology is successful in a solution space that is now three times as large as Voyager 1. Surprisingly, PSO is again able to identify favorable solutions early on in most of the trials, with no trials returning trajectories that have significantly different flyby scenarios as compared to that of the Voyager 2 mission model. Figures 5.5-5.7 show the two solutions side by side, with the black PSO trajectory laying closely on top of the bright blue mission model trajectory.

Table 5.4: Comparison of results between optimal case and Voyager 2 mission ($N_{FB} = 3$).

| Mission | Flyby | Date | $\Delta v_{s_N}\,(km/s)$ | $r_p\,(km)$ | $\Delta V_L\,(km/s)$ | $\Delta V_{FB}\,(km/s)$ | $\Delta V_A\,(km/s)$ | $J\,(km/s)$ |
|---|---|---|---|---|---|---|---|---|
| PSO | Jupiter | 07/14/1979 | $1.677 \times 10^{-5}$ | $709,578$ | 10.1406 | 11.6395 | 16.7552 | 26.9070 |
| | Saturn | 08/31/1981 | 0.0112 | $157,238$ | – | 14.5320 | – | – |
| | Uranus | 01/25/1986 | $6.3385 \times 10^{-5}$ | $106,993$ | – | 5.8740 | – | – |
| Voyager 2 | Jupiter | 07/09/1979 | 0.0310 | $701,801$ | 10.1186 | 11.7055 | 16.7360 | 26.9329 |
| | | | | Real [38]: $721,670$ | | | | |
| | Saturn | 08/26/1981 | 0.0378 | $341,099$ | – | 14.5576 | – | – |
| | | | | Real [38]: $161,000$ | | | | |
| | Uranus | 01/24/1986 | $5.3236 \times 10^{-4}$ | $107,039$ | – | 5.8766 | – | – |
| | | | | Real [38]: $107,000$ | | | | |

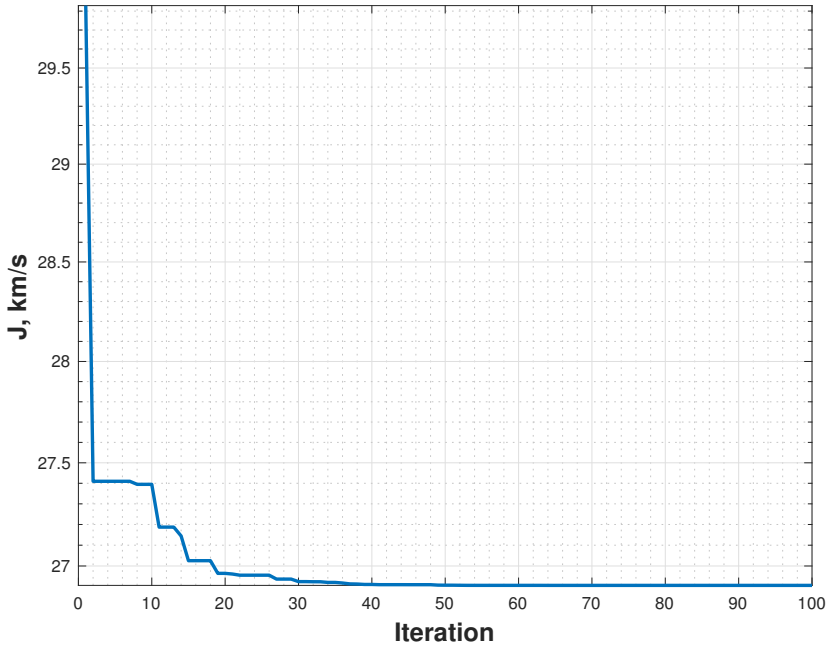


Figure 5.4: PSO cost function convergence vs. iteration number for Voyager 2 (log scale y-axis).

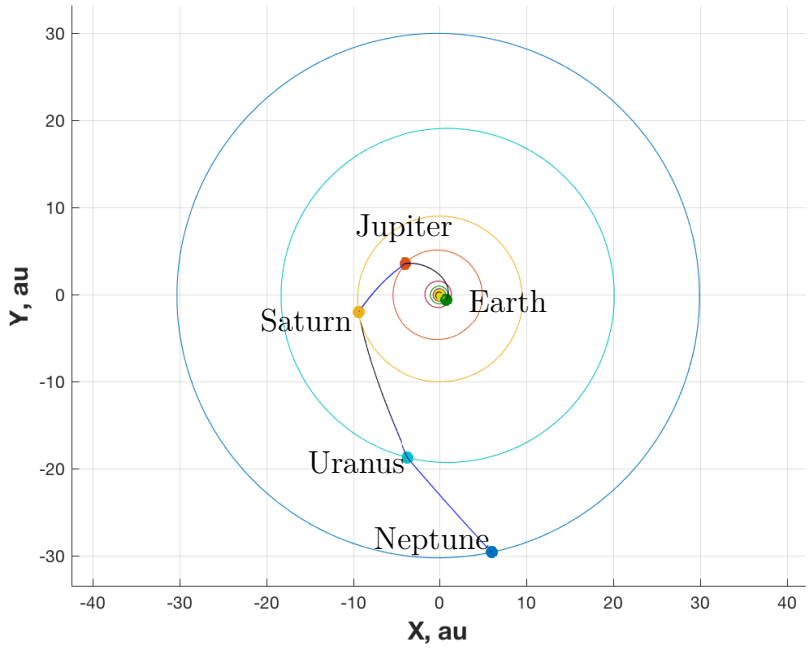


Figure 5.5: The optimal result from PSO vs. the actual Voyager 2 mission dates (SICF).

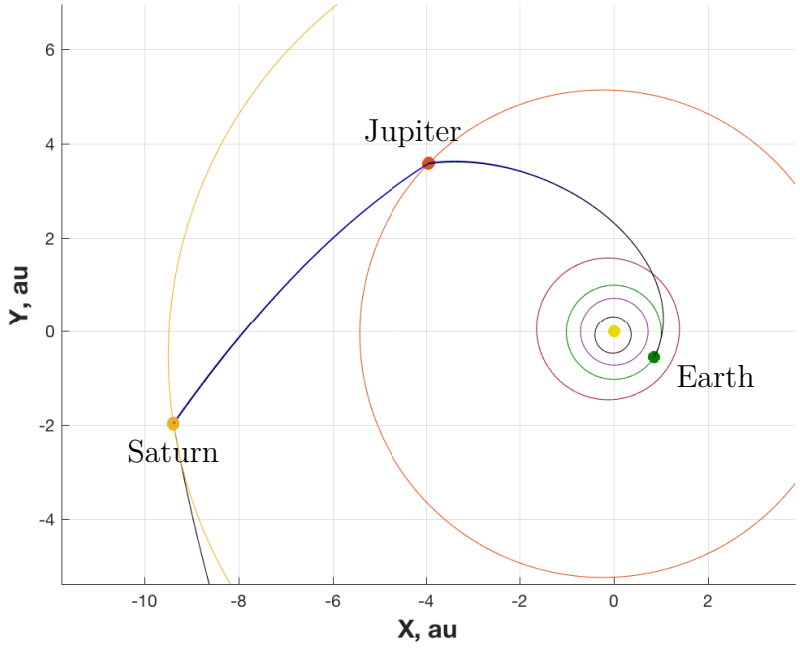


Figure 5.6: The optimal result from PSO vs. the actual Voyager 2 mission dates (closer look at inner solar system view, SICF).

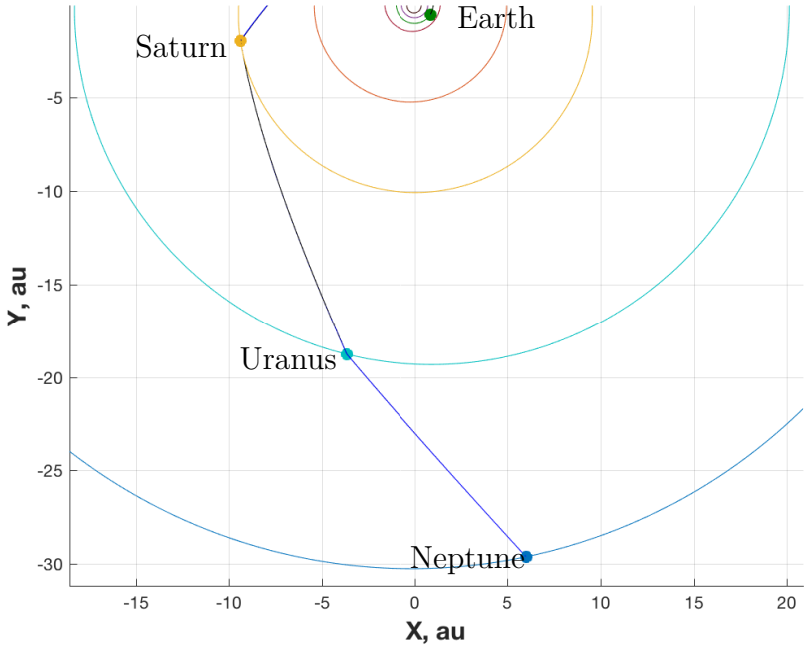


Figure 5.7: The optimal result from PSO vs. the actual Voyager 2 mission dates (closer look at outer solar system view, SICF).

### 5.2.3 Cassini Case

Cassini is selected as the third trajectory design case and provides yet another opportunity to increase the number of decision variable for the MGA problem ($N_{FB} = 4$). Cassini recently finished its lifetime of science research by taking a final plunge into the destination planet, Saturn. The interplanetary trajectory arrived at Saturn on July 1st, 2004. Originally, Cassini launched from Earth on October 15th, 1997 and required four flybys in series as: Venus on April 26th, 1998 (at an altitude of 284 kilometers), Venus again on June 24th, 1999 (altitude unavailable), Earth on August 18th, 1999 (at an altitude of 1175 kilometers), and Jupiter on December 30th, 2000 (at an altitude of 9,700,000 kilometers). One key distinction for this mission is that it involves one targeting maneuver that was executed in order to better phase the second encounter with the planet Venus. The addition of deep-space maneuvers is not included as a part of the MGA problem formulation, and is therefore neglected from the model.

The best result of this mission design is found after running 25 trials of PSO. For the first few trials (5-10 of them), the solution space is reduced by enforcing stricter bounds and slowly increasing them to the desired values. The bounds are chosen to start as 10 days before and 10 days after the actual mission flyby dates. As success is encountered, the solution space is expanded to the final bounds of 10 days after launch date, 10 days before arrival date, and 10 days after or before any flyby. Eventually, the same bounds as applied to Voyager 1 and Voyager 2 are able to return an optimal trajectory.

Although the solution space was expanded, the PSO solution does not fall exactly in line with that of the modeled mission. This behavior does not come as a surprise, since the deep-space maneuver previously mentioned is not included as part of the trajectory model. One key takeaway from this mission case is that the flyby distances for the modeled trajectory violate the periapse constraint. Interestingly enough, PSO finds a way to identify a more suitable trajectory option for the given MGA problem model. PSO identifies a potential trajectory that alters the dates of the first two flybys enough to meet all periapse constraints. Effectively, PSO identifies a way of incorporating a larger synergetic maneuver in place of completing a deep-space maneuver.

The solution takes 100 iterations, with a swarm population of 50 particles, and elapses 62.36 seconds of wall clock time. The algorithm has similar convergence compared against that of the Voyager 2 mission, as shown in Figure 5.4. The

indication from this result is that a fourth decision variable does require more trials of PSO, but does not stop the algorithm's ability to identify an optimal solution. The final PSO solution has free selection of the Julian dates for the four flyby encounters from 10 days after launch date, 10 days before arrival date, and 10 days after or before any flyby. The optimal flyby date for the first encounter of Venus as viewed by the optimizer is March 27th, 1998 with an altitude of 5998.20 kilometers. The optimal flyby date for the second encounter with Venus is chosen as June 3rd, 1999 at an altitude of 8352.54 kilometers. The optimal flyby date for Earth is selected as August 4th, 1999 at a closest approach radius of 500.00 kilometers.

For direct comparison, the actual dates for Cassini are passed through the dynamic model, where the altitude of the Venus flybys are 885 kilometers and -4349 kilometers (respectively), the altitude of the Earth flyby is -1273 kilometers, and the altitude of the Jupiter flyby is 7,305,377 kilometers. The flyby manuevers here are a mix of free-flight type maneuvers and more significant synergetic maneuvers. The results of Table 5.5 show that Cassini's actual mission flown dates show results for both types of flybys. The PSO solution shares some characteristics with the modeled solution in places. However, they have a distinct separation before and after the date where deep-space targeting maneuver is supposed to be executed. For the modeled trajectory, periapse violations occur. However, there are no violations of the periapse radius for the PSO solution.

This mission shows that obtaining results for four decision variables using PSO on the MGA problem is feasible. However, this mission highlighted some weaknesses in the modeling techniques that may be improved with higher fidelity considerations in the future. One takeaway from this mission case is that the inner planets display much higher sensitivity to the timing of flybys in the MGA problem. The inner planets rotate around in their respective orbits much faster than the outer planets, leading to more opportunities for potential flybys. However, this larger range of options comes with a price. The inner planets are also smaller in size and contribute less energy from a given flyby than a flyby of a much larger, outer planet does. With smaller size also comes the complication that the radius of periapse often ends up closer to the body during flyby, in order to obtain the same perturbing effect from the gravitational assist. A positive takeaway from this mission case is that PSO is again able to identify favorable solutions early on in a large portion of the trials. Notably PSO ends up returning trajectories that have fairly different flyby scenarios as compared to that of the Cassini mission model. The variation between

the two solutions is prevalent for the flyby encounter of Venus. Figures 5.9-5.11 show the black PSO trajectory versus the bright red mission model trajectory. The difference seen here from neglecting a single deep-space targeting maneuver was significant enough to indicate that further validation from other MGA missions like Galileo and MESSENGER would not be of interest, until future models could also support deep-space targeting maneuvers.

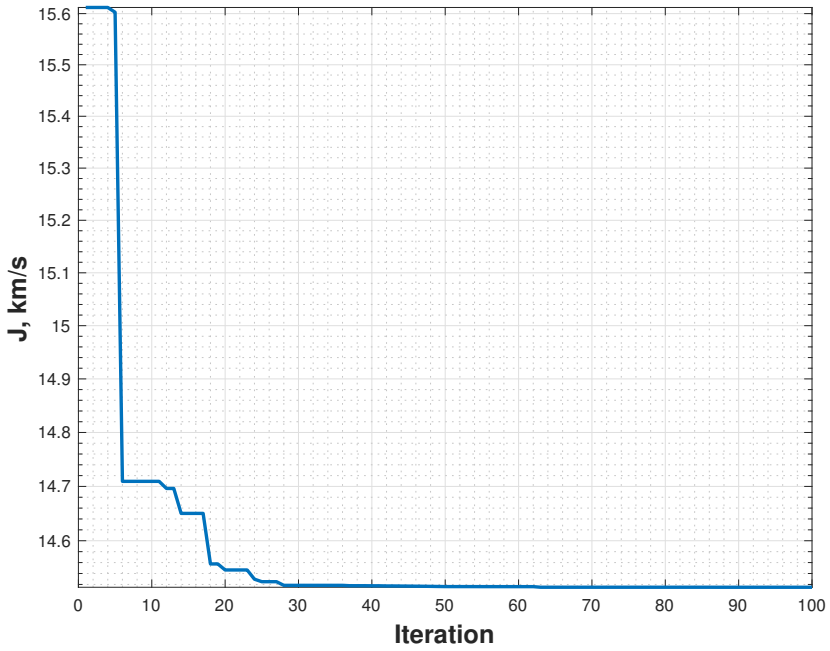


Figure 5.8: PSO cost function convergence vs. iteration number for Cassini (log scale y-axis).

Table 5.5: Comparison of results between optimal case and Cassini mission ($N_{FB} = 4$).

| Mission | Flyby | Date | $\Delta v_{s_N}\,(km/s)$ | $h_p\,(km)$ | $\Delta V_L\,(km/s)$ | $\Delta V_{FB}\,(km/s)$ | $\Delta V_A\,(km/s)$ | $J\,(km/s)$ |
|---|---|---|---|---|---|---|---|---|
| PSO | Venus | 03/27/1998 | 0.7763 | 5998.20 | 2.9370 | 6.0634 | 2.2532 | 14.5149 |
| | Venus | 06/03/1999 | 0.0446 | 9352.54 | – | 8.7319 | – | – |
| | Earth | 08/04/1999 | 5.4437 | 500.00 | – | 10.5089 | – | – |
| | Jupiter | 12/17/2000 | $4.1246 \times 10^{-6}$ | $9,481,590$ | – | 5.3132 | – | – |
| Cassini | Venus | 04/26/1998 | 0.4751 | 885 | 4.4550 | 6.8959 | 6.2458 | $5.6424 \times 10^3$ |
| | | | | Real [38]: 284 | | | | |
| | Venus | 06/24/1999 | 1.4946 | $-4349$ | – | 12.5015 | – | – |
| | | | | Real [38]: $N/A$ | | | | |
| | Earth | 08/18/1999 | 8.6197 | $-1273$ | – | 15.3358 | – | – |
| | | | | Real [38]: 1175 | | | | |
| | Jupiter | 12/30/2000 | 0.2913 | $7,305,377$ | – | 2.8505 | – | – |
| | | | | Real [38]: $9,700,000$ | | | | |

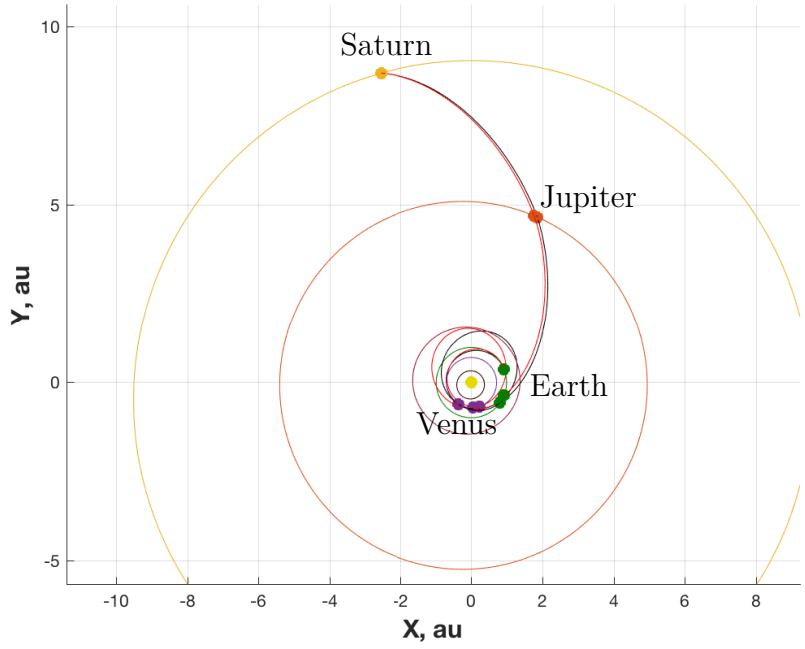


Figure 5.9: The optimal result from PSO vs. the actual Cassini mission dates (SICF).

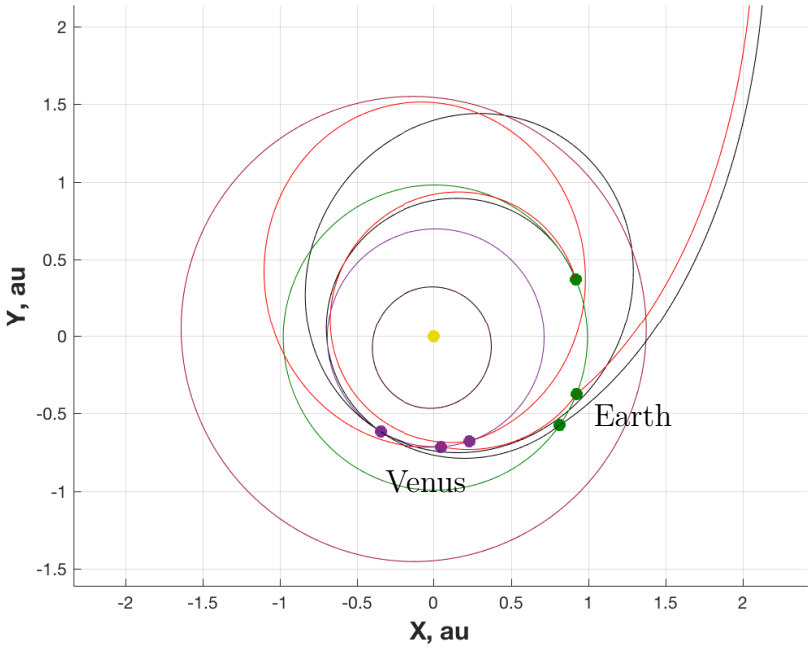


Figure 5.10: The optimal result from PSO vs. the actual Cassini mission dates (view near Earth and Venus, SICF).

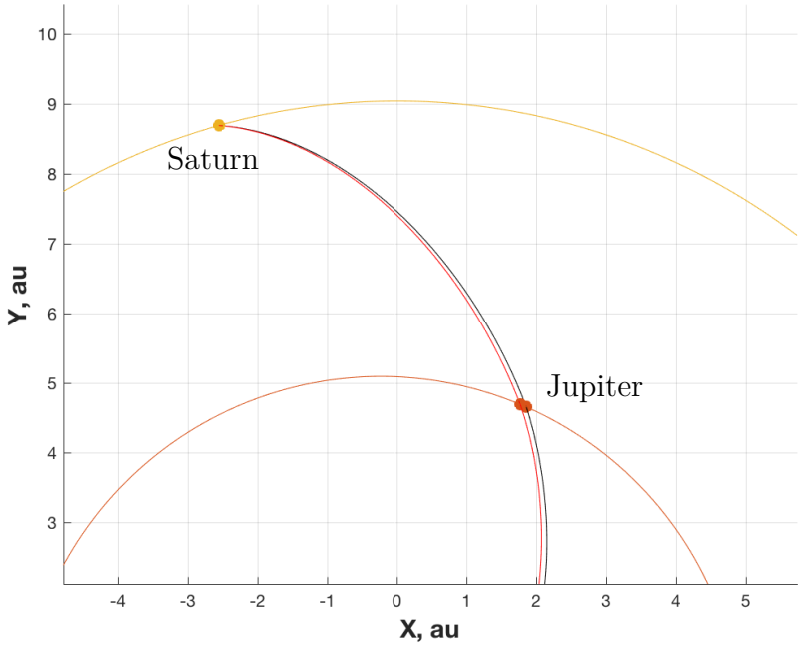


Figure 5.11: The optimal result from PSO vs. the actual Cassini mission dates (view near Jupiter and Saturn, SICF).

### 5.2.4 Design of a Mission to Saturn

The last trajectory design case is a novel mission design from Earth to Saturn. The proposed launch date from Earth is that of August 10th, 2018. Both a direct route and a MGA route are considered. The MGA route aims to arrive at Saturn by first flying by Venus and then Jupiter ($N_{FB} = 2$). Two preferable arrival options are also proposed, the first being a solution corresponding to a time of flight of 3 years (arrival on August 10th, 2021) whereas the second is solution corresponding to a time of flight of 4 years (arrival on August 10th, 2022).

The direct trajectories to Saturn pale in comparison to the MGA trajectories for both the 3 year and 4 year arrival cases. A direct mission to Saturn is not possible given the large propellant cost required. In addition, the trajectory for the 3 year case involves a highly elliptical orbit that passes extremely close to the Sun, which would not be practical for many reasons (such as thermal requirements). However, the MGA trajectories are much more feasible, and could potentially provide scientific survey opportunities as the flyby encounters of Venus and Jupiter are completed. Here, the benefit of MGA trajectories is clear, as they open up

opportunity for missions that are not normally feasible in this design case.

The best MGA results of this mission design is found after running 10 trials of PSO and is presented here. The solution took 100 iterations, with a swarm population of 50 particles, and elapsed 59.55 seconds for the 3 year solution and 58.01 seconds for the 4 year solution. The algorithm provides similar convergence behavior to that previously seen in mission cases 1-3, and this is shown in Figures 5.12-5.13.

The upper and lower bounds for the two flyby dates follow the methodology previously applied to mission cases 1-3 as well, with PSO freely selecting from 10 days after launch date, 10 days before arrival date, and 10 days after or before any flyby. For the 3 year solution, the optimal flyby date for Venus as viewed by the optimizer is January 9th, 2019 with a flyby altitude corresponding to 500.00 kilometers. The optimal flyby date for Jupiter is chosen as March 8th, 2020 at a flyby altitude of 1,003,840 kilometers. As for the 4 year solution, the optimal flyby date for Venus changed to January 10th, 2019 at an altitude of 500.00 kilometers. A more significant change to the flyby date of Jupiter is present with the date now shifting to June 3rd, 2020 with altitude of 2,255,735 kilometers in this case.

Design of this mission confirms that the performance for the PSO algorithm on two decision variables holds consistent with those results seen for other quantities of decision variables. Here, PSO is able to quickly identify favorable solutions early on in most of the trials. Figures 5.16-5.18 show how much difference an additional year in total mission time makes, even for a mission traveling to an outer planet. The propellant savings for a mission that requires one extra year are significant and is a trade-off that mission planners have the ability to explore with this method for designing trajectories.

Table 5.6: Comparison of MGA and direct mission to Saturn taking 3 years vs. 4 years ($N_{FB} = 2$).

| Mission | Flyby | Date | $\Delta v_{s_N}\,(km/s)$ | $h_p\,(km)$ | $\Delta V_L\,(km/s)$ | $\Delta V_{FB}\,(km/s)$ | $\Delta V_A\,(km/s)$ | $J\,(km/s)$ |
|---|---|---|---|---|---|---|---|---|
| PSO (MGA), 3 year | Venus | 01/09/2019 | 7.6036 | 500.00 | 4.6152 | 15.8691 | 10.1156 | 28.5122 |
| | Jupiter | 03/08/2020 | $6.6145 \times 10^{-10}$ | $1,003,840$ | – | 16.2934 | – | – |
| Direct, 3 year | – | – | – | – | 48.7960 | – | 12.9436 | 61.7396 |
| PSO (MGA), 4 year | Venus | 01/10/2019 | 6.8052 | 500.00 | 4.7584 | 12.0904 | 6.5614 | 21.3501 |
| | Jupiter | 06/03/2020 | $2.6759 \times 10^{-6}$ | $2,255,735$ | – | 9.7864 | – | – |
| Direct, 4 year | – | – | – | – | 48.6330 | – | 9.9474 | 58.5803 |

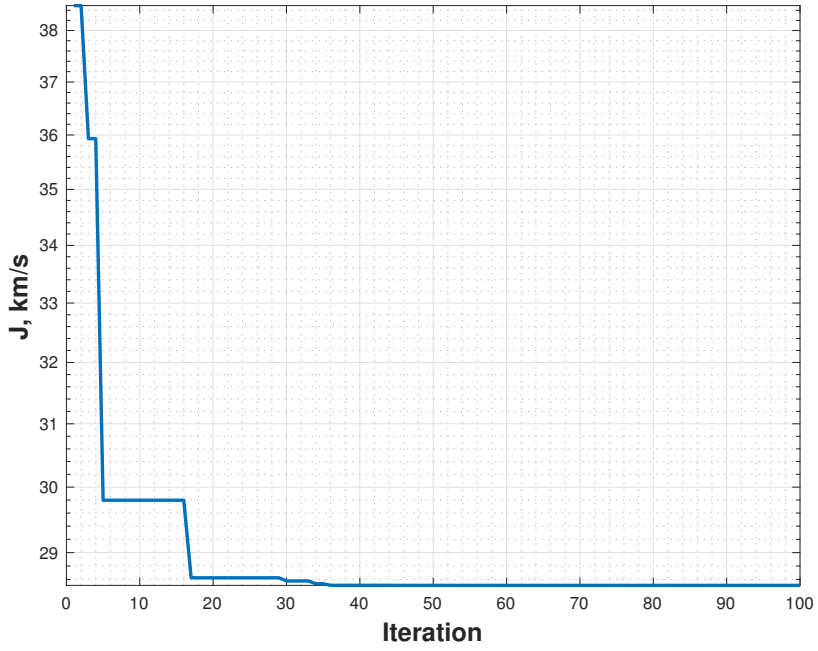


Figure 5.12: PSO cost function convergence vs. iteration number for the chosen mission to Saturn taking 3 years (log scale y-axis).

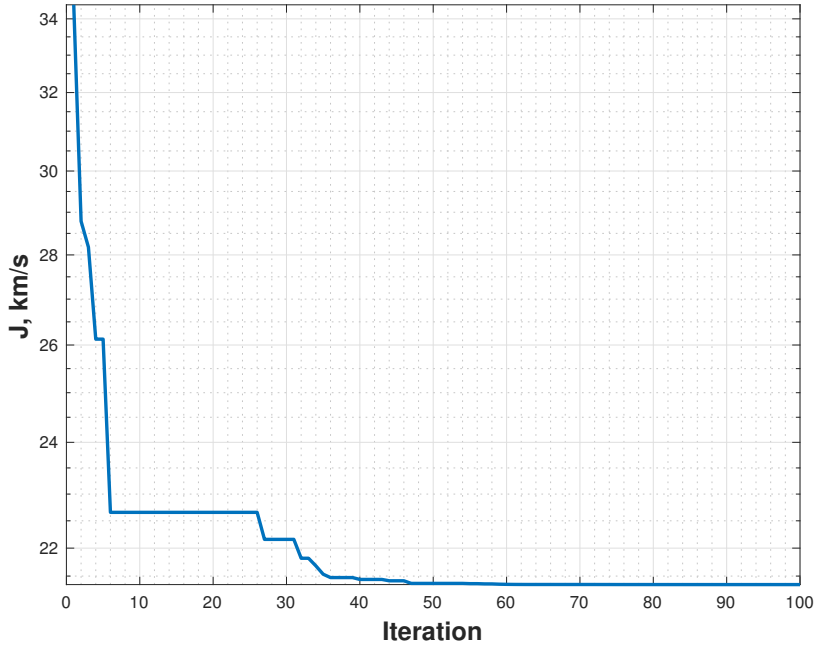


Figure 5.13: PSO cost function convergence vs. iteration number for the mission to Saturn taking 4 years (log scale y-axis).

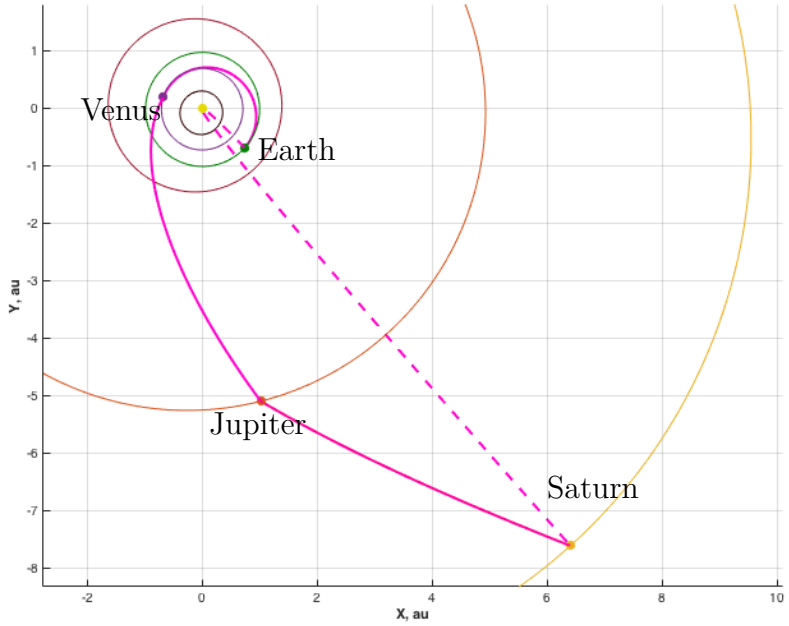


Figure 5.14: The optimal result from PSO for the 3 year mission vs. a direct transfer to Saturn (SICF).

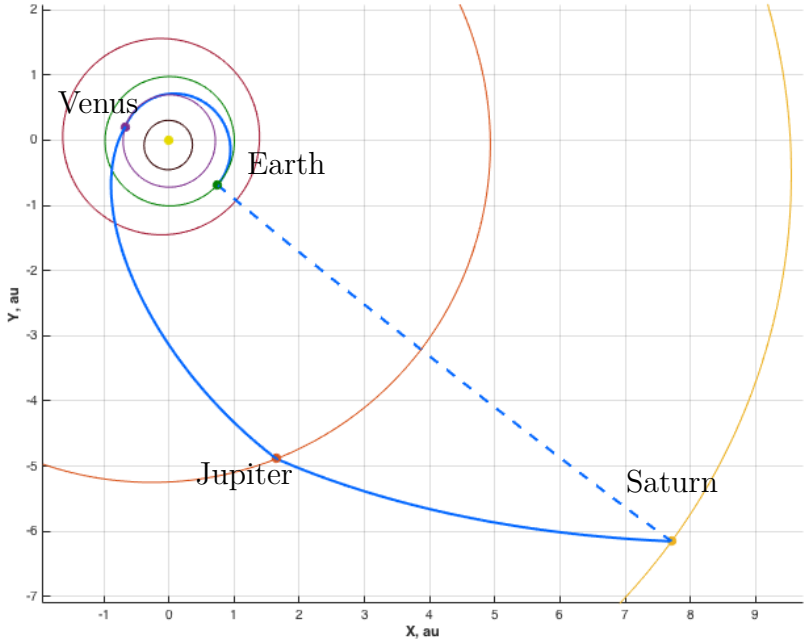


Figure 5.15: The optimal result from PSO for the 4 year mission vs. a direct transfer to Saturn (SICF).

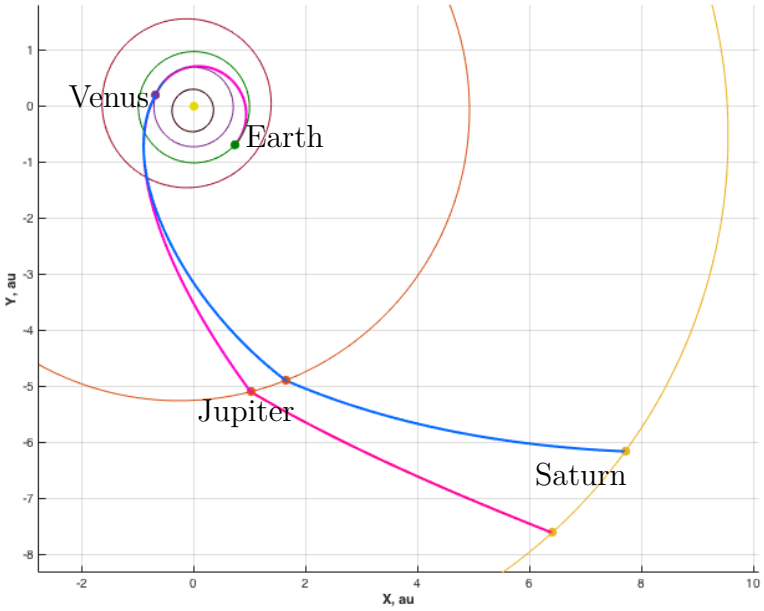


Figure 5.16: The optimal result from PSO for the 3 year mission vs. the 4 year mission to Saturn (SICF).

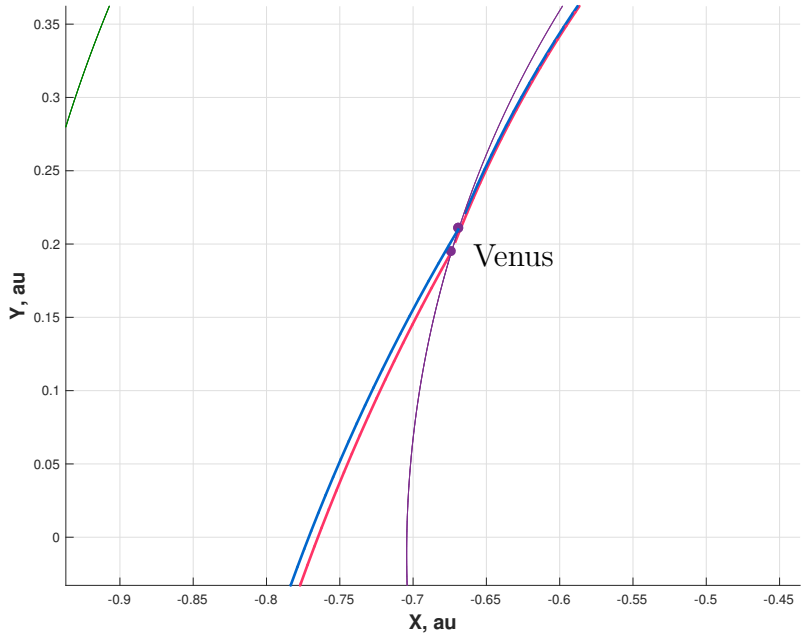


Figure 5.17: A closer look at the Venus flyby encounters in the heliocentric frame for the 3 year and 4 year missions to Saturn (SICF).

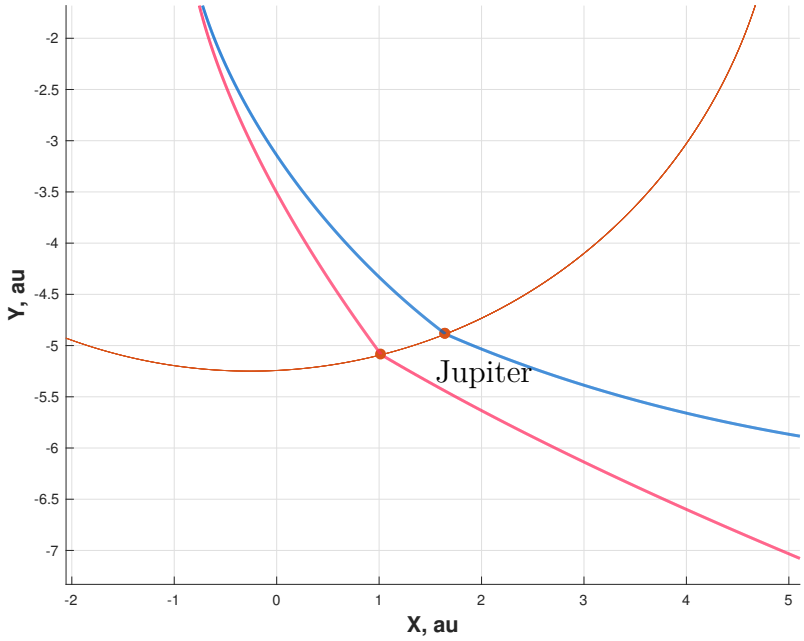


Figure 5.18: A closer look at the Jupiter flyby encounters in the heliocentric frame for the 3 year and 4 year missions to Saturn (SICF).

## 5.3 Qualitative Findings

The PSO algorithm is chosen for this research due to its ability to search large trade spaces in a computationally efficient manner. Here, the PSO algorithm delivers that benefit by searching the MGA problem tradespace for flyby dates in a reasonable amount of time, often around one to two minutes of execution time. In addition, the computational efficiency of the algorithm and its ease of implementation make it attractive for applications such as preliminary mission design. Although there is no guarantee that the PSO results here are globally optimal results, they align well with previous mission data and basic mathematical models for these missions. The MGA problem is one that does not lend itself to a closed form analytic solution, so verification against previous MGA mission design is a logical first place to test the algorithm and its performance. Although assumptions regarding modeling details show a potential to change the accuracy of the PSO solutions, it seems that the solutions found by the PSO algorithm have the ability to compare against

well known trajectories from Voyager 1, Voyager 2, and Cassini. If higher fidelity modeling is desired, it seems PSO may still perform well for the task. No major computational bottlenecks are discovered as a part of this research, although the method may prove even faster in alternative programming languages.

One potential area of further research is that of multi-revolution solutions. Especially when weighing trajectory options for flybys involving inner planets, the multi-revolution solutions may prove more efficient in terms of a cost function. The trade-off between multi-revolution solutions is most likely strongest for trajectories involving the inner planets. The PSO method proposed performs quite well on trade spaces involving the outer planets, potentially due to the larger times of flight associated with traveling to the outer planets. Their sensitivity to small changes in flyby dates seems to be lesser and more gradual in terms of a propellant-based cost function. The number of local minima in the trade space involving the outer planets also appears to be lesser. For trials of PSO involving missions to outer planets (Voyager 1 and Voyager 2 as examples), identical solutions can be repeated over and over again with very little variability in the mission's individual flyby dates.

Lastly, the synergetic capability performs well and simplifies as expected to cases of free-flight gravity assist maneuvers. One key finding of the present research is that the synergetic flyby analysis allows for many more trajectory options to become feasible for small costs in terms of propellant usage. Trajectories that may normally be neglected due to a mismatch in hyperbolic excess velocity magnitude at a flyby planet are identified as feasible here. Additionally, synergetic flybys afford a chance to exceed the upper bounds for heliocentric changes in velocity that exist only for free-flight gravity assist maneuvers, allowing even more trajectories between planets to become feasible for mission planners.

# Chapter 6
# Conclusions

## 6.1 Addressing Research Questions

Originally in the first chapter of this thesis, a set of fundamental research questions were presented. The goal of this thesis is to answer those research questions by obtaining results and quantitative findings. Those results and findings then serve to support the qualitative conclusions that properly answer the questions posed.

**Question 1:** How does Particle Swarm Optimization perform for the multiple gravity assist trajectory design space?

**Answer 1:** Particle Swarm Optimization performs well in the MGA problem design space as evidenced by the results shown for Voyager 1, Voyager 2, and Cassini. Further, the method holds up well when tasked to identify potentially useful trajectories for an entirely new mission never conceived before. Bessette [20] and Bessette and Spencer [21] had first examined this type of problem with only one free-flight flyby maneuver, but under expansion of this problem to multiple synergetic gravity assist maneuvers the results are encouraging. One key note to remember is that the results by PSO are only as good as the model can allow them to be. For that reason, higher fidelity problems may require research in the future. However, as a starting point the results produced here within this thesis show that a higher fidelity investigation into the MGA problem is worthwhile.

**Question 2:** What benefits and downfalls exist when formulating the scheduling problem for gravitational assist maneuvers as a multivariate optimization problem minimizing propellant?

**Answer 2:** Formulating the scheduling problem into a multivariable optimization problem proves beneficial in two distinct ways.

First, computational efficiency when investigating the trade space for flybys is present, meaning that a reasonable answer to the optimization problem is only a few minutes away for a mission designer. The computational savings here are vast when compared to the alternative description, which requires solving the problem incrementally and investigating solutions in a tree-search structure. Here, there is a tendency for the size of the solution space to become a challenge, as each branch requires many permutations of decisions, especially as the number of flybys increases.

Second, there exists new and potentially attractive solutions to the MGA problem when allowing flyby encounters to include synergetic capabilities. In past research, many have opted to only consider free-flight maneuvers, as there appeared to be potentially infinite possibilities for different amounts of delta-v that powered flybys could take on for the MGA problem. By formulating the problem as a multivariable optimization as in this thesis, there exists only one synergetic flyby at each planetary encounter that satisfies Lambert's problem leading into and out of the encounter.

Although there are two significant benefits to formulating the problem in this way, there exists also a downside. There is a limited fidelity available for the MGA problem with this method. The linked conics model cannot easily be transformed into a patched conics model. The reason for this is due to the fact that each flyby involves a finite amount of time for the spacecraft to travel from one edge of the sphere of influence of a body to the other edge. The time of flight from one edge to edge in turn affects the Lambert solution. However, the time of flight from an initial orbit to a final orbit must be known beforehand, in order to solve for the unique velocities required at the start and end of the transfer trajectory. With a linked conics multivariable formulation, the time of flight is simply from heliocentric body 1 to heliocentric body 2. However, the patched conics solution requires a time of flight from heliocentric body 1 to heliocentric body 2, the time of flight spent inside of the sphere of influence of body 1, and also the time of flight spent inside of the sphere of influence of body 2. It is not possible to determine the latter two times of flight without first knowing the velocities

required at the spheres of influence of body 1 and body 2 (found by first solving for the Lambert transfer trajectory). Therefore, a circular logic exists here, and the patched conics model requires a reformulation of the MGA problem before a solution is obtainable.

**Question 3:** Can previous mission results be either confirmed or improved using this approach?

**Answer 3:** Previous missions are confirmed with reasonable accuracy using PSO on the Voyager 1 and 2 missions. The PSO Cassini solution shows a slight difference in some parts of the trajectory as compared to the real mission. This variation is due to the fact that the real mission had a functionality that the MGA problem formulation presented here does not capture in the same way, because deep-space maneuvers are not modeled. However, PSO manages to identify an interesting alternative using a synergetic gravity assist approach instead of a deep-space maneuver.

## 6.2 Future Research Direction

The fundamental research questions are answered with the model and analysis implemented by this thesis. Now that the research presented here has been conducted, there are new investigations that are worth considering for future research direction.

In particular, formulating the MGA problem in a way that patched conics can be modeled is of interest for increasing the level of fidelity for mission design. There may be a way to introduce PSO into that formulation by computing full solutions to the scheduling type problem. Each solution might be propagated along sequentially from Earth launch to each particular flyby encounter. Eventually, the mission trajectory would cross the desired planet's orbital path with respect to the Sun. At that point, each solution could be evaluated by a cost that represents the difference between that solutions actual arrival location versus the planet's location. Lower cost would mean that the planet and the spacecraft coincide at the arrival point, and higher cost would mean they deviate from one another. Not every solution would necessarily achieve a trajectory that would reach the proper location of the arrival planet, however PSO could be used to find and favor trajectories that satisfy this condition. Although PSO does not formally enforce equality constraints in

optimization problems, if the right cost function could be developed, there exists the possibility that a solution intercepting the arrival planet could be found. PSO performed a very similar action in the present research, by favoring trajectories that resulted in flybys greater than an altitude of 500 kilometers above the planet surfaces (with no violations found).

An alternative investigation that may be worth conducting in the future is one that examines the potential to allow PSO to choose more aspects of the MGA problem formulation presented here. The sequencing problem was not tackled as part of this research, and instead a sequence of bodies was prescribed or already known for the missions examined here. However, the optimization problem expands as the number of bodies or the choice of planets is considered when determining which sequences perform best to get from launch planet to arrival planet. For example, the departure and arrival dates could be included as decision variables themselves. This would allow mission designers to place upper and lower bounds on these dates and vary the total time of flight of the missions that they design. Along those same lines, the ability to include multiple revolution orbits for Lambert solutions could be investigated. An additional decision variable could be introduced for each Lambert trajectory. This new set of decision variables could range as integers from zero to a desired number of revolutions to be considered. PSO could even potentially be used to expand and start towards solving the sequence of planets required to execute a mission. In order to do such a thing, PSO could be given the ability to choose the planets that a mission would execute flybys around. Again, integer numbers representing each planet, 1 through 8 would be an easy way to represent this choice. The planet identity for each flyby maneuver would then become a decision variable. In order to take a slightly different approach to the sequencing problem for MGA, it could also be possible to allow the total number of flybys that a mission would execute to be an integer decision variable. Users could specify lower and upper bounds on this integer value. Note that if new decision variables are added to the definition of a particle for PSO, that change may require an alteration to the number of iterations or the number of particles used in order to compensate for this change. One thing to consider, if convergence is not as fluent under larger numbers of decision variables, is changing the type of PSO algorithm used. There are alternative versions where stagnation of particles is handled by restarting a certain number of particles in randomized spots in the solution space in an effort to pull the swarm away from local minima that are encountered.

Beyond just changing the number of decision variables that PSO has control over, there also exists the possibility to change or alter the cost function that PSO uses to evaluate the mission trajectories. Here, the cost function is based on the propellant consumed by the spacecraft as well as the proximity that the spacecraft has with respect to each flyby planet. However, this is not the only cost function that could be possible. Additionally, there exists the opportunity to apply coefficients or weights to each of the changes in velocity of the cost function used by this thesis to uniquely emphasize launch maneuvers, flyby maneuvers, or arrival maneuvers with respect to one another.

In terms of the model of the MGA problem, there exists the opportunity to include deep-space maneuvers as an option for trajectories. The number of deep-space maneuvers and their locations would most likely need to be implemented as decision variables, as a deep-space maneuver may not always be required for any given mission. A related analysis that might be of interest is to examine the ability that synergetic flybys provides for amplifying the delta-v applied in the flyby planet's frame. In each of the cases examined through this research, the delta-v expelled around the flyby planet appeared to be amplified by some value greater than unity when compared to the corresponding heliocentric delta-v obtained by the flyby encounter. The amplification depends on the incoming velocity vector, outgoing velocity vector, and the planet that the flyby is to occur. Quantifying the amplification behavior of the synergetic gravity assist would be useful in order to give mission planners more knowledge when choosing which planets to target for flybys.

A final investigation that would be useful to conduct would be one changing the heuristic optimization algorithm. For this research, PSO was selected due to its performance as studied in the single gravity assist optimization problem. However, differential evolution has been seen to have similar performance [20, 21]. A useful study could be one comparing the two algorithms again, but in the MGA problem space to see if similar results are obtained.

Lastly, as more decision variables are chosen by PSO there will need to be more particles (solutions) computed for each individual iteration to properly search the trade space. Although no computational bottlenecks were encountered through the work presented here, there exists a potential for the number of Lambert solutions to radically increase as more decision variables are taken on. In the event that the Lambert solution starts to slow down the computation time, a researcher

might consider using a method to approximate Lambert's problem such as the linearization approach taken by McMahon and Scheeres [39]. That method could reduce computation time for that calculation of Lambert's problem, while still returning enough detail about solutions find near optimal solutions. The near optimal solutions could then be used as a starting point in higher fidelity models that are capable of refining the solutions further.

# Appendix
# MATLAB Program Description

## 1 Program Files

The research that is presented in this thesis required creating several ".m" files in MATLAB for calculation and visualization of results. The names of each file and their purpose are summarized:

## 2 Function Files

The complexity of the program is reduced by using function files in order to segment routines that execute related operations or series of repetitive commands.

### 2.1 `cartesian_orbital_EOMs.m`

**Details:** A function containing state-space representation of the two-body problem equations of motion.

**Purpose:** Numerical integration of initial state vector for planets and Lambert trajectories for verifying calculations and plotting purposes.

**Inputs:** State at previous time, time step to next desired state.

**Outputs:** Derivative information to determine state at a desired time .

### 2.2 `fast_solar_system.m`

**Details:** A function controlling the propagation of ephemeris data for solar system that utilizes Lagrange coefficients.

**Purpose:** Make the function calls to propagate all bodies in the solar system individually via Lagrange coefficients.

**Inputs:** Julian date at an epoch, epoch ephemeris data, Julian date for desired ephemeris data, gravitational parameter.

**Outputs:** Ephemeris data at new Julian data for all of solar system.

### 2.3 `function_evaluation_MGA.m`

**Details:** A function controlling the entire function evaluation of dynamics for the PSO optimization.

**Purpose:** Organize all of the dynamics required into one routine, returning only the calculated values of interest.

**Inputs:** Julian dates for flyby encounters, all physical constants for each body of interest for solution, a schedule of epoch date for ephemeris, launch date, arrival date, a sequence of planets to be visited (integers), all necessary ephemeris data.

**Outputs:** Cost function value of mission, results values of interest (such as delta-v's, radii of periapse, etc.), a mission plan summary of bodies and corresponding date(s) of visitation.

### 2.4 `glambert.m`

**Details:** A function that solves for Lambert trajectories between two specified position vectors, provided by John's Hopkins Applied Physics Lab (APL).

**Purpose:** Determine the trajectories between flybys in the heliocentric frame (SICF).

**Inputs:** Gravitational parameter, state vector (position, velocity) at initial point in space, state vector (position, velocity) at final point in space, time of flight taken between two points in space, number of revolutions desired.

**Outputs:** Velocity vector required to enter onto transfer orbit, velocity vector required to leave off transfer orbit.

### 2.5 `numerical_orbit.m`

**Details:** A function controlling the call to `ode45.m`, numerically integrating an orbit.

**Purpose:** Organize and automate a routine that does all required commands necessary to integrate trajectories.

**Inputs:** Initial conditions for integrating state vector over time, desired total integration time.

**Outputs:** State vector of trajectory over total integration time.

### 2.6 `particle_swarm_optimization.m`

**Details:** A function containing the algorithm required to execute Particle Swarm Optimization (PSO).

**Purpose:** Heuristic algorithm that selects Julian dates for flybys of a mission and quickly evaluates their cost in search of an optimal solution.

**Inputs:** Problem information (number of free decision variables, lower and upper bounds on free variables, function evaluation information), parameters for PSO algorithm (number of iterations, number of particles, the coefficient values) .

**Outputs:** Results of optimization algorithm (global best solution, cost of global best solution).

### 2.7 `propagator.m`

**Details:** A function containing the Lagrange coefficient analysis required to propagate an orbit through time.

**Purpose:** A fast alternative method for calculating the state of all planetary orbits in the solar system in substitution of `planetEphemeris.m`.

**Inputs:** Time of desired state from initial known state, initial position vector, initial velocity vector, gravitational parameter.

**Outputs:** Position vector at desired time, velocity vector at desired time.

### 2.8 `solar_system.m`

**Details:** A function controlling the propagation of ephemeris data for solar system that utilizes the Aerospace toolbox's `planetEphemeris.m`.

**Purpose:** Make the function calls to propagate all bodies in the solar system individually via `planetEphemeris.m`.

**Inputs:** Desired Julian date for ephemeris data.

**Outputs:** Ephemeris data at desired Julian data for all of solar system.

### 2.9 `synergetic_flyby.m`

**Details:** A function containing analysis for a synergetic flyby.

**Purpose:** Calculate the required trajectory details for a given set of hyperbolic excess velocity vectors into and out of the sphere of influence (SOI) of a flyby planet.

**Inputs:** Planet physical constants, hyperbolic excess velocity vector into SOI (in terms of PRCF), hyperbolic excess velocity vector out of SOI (in terms of PRCF)

**Outputs:** Turn angle, radius of periapse, delta-v required at periapse, number of iterations in multivariate Newton-Raphson method, semi-major axes (both incoming and outgoing hyperbolas), eccentricities (both incoming and outgoing hyperbolas).

### 2.10 `visualization.m`

**Details:** A function containing all plotting commands to create a figure of the trajectory for a mission.

**Purpose:** Organize all function calls and create a routine that produces a visualization of a trajectory for a mission.

**Inputs:** Ephemeris data for all bodies plotted, sequence of planets to be visited, velocities for all points of mission, times of launch, arrival, and flyby encounter(s), and color scheme for all curves to be plotted.

**Outputs:** A figure with full mission trajectories and all planetary orbits, state vector at all times of integration for each Lambert trajectory required by the mission.

# 3 Script (Main) Files

In an effort to segment analysis for different missions, individual missions are ran with independent main files that are operated as scripts in MATLAB. The mission scripts contain unique dates and sequences of planets. Each mission script also contains a trajectory that is evaluated by the dynamic model using the actual dates flown by the mission (when applicable) for comparison with a PSO generated solution.

## 3.1 `Main_File_Cassini.m`

**Details:** A script containing all definitions of dates, relevant mission information (sequence of bodies, real mission data for comparison, etc.), and PSO parameter definitions.

**Purpose:** Organize all function calls for a mission into one script for Cassini.

## 3.2 `Main_File_Voyager_1.m`

**Details:** A script containing all definitions of dates, relevant mission information (sequence of bodies, real mission data for comparison, etc.), and PSO parameter definitions.

**Purpose:** Organize all function calls for a mission into one script for Voyager 1.

## 3.3 `Main_File_Voyager_2.m`

**Details:** A script containing all definitions of dates, relevant mission information (sequence of bodies, real mission data for comparison, etc.), and PSO parameter definitions.

**Purpose:** Organize all function calls for a mission into one script for Voyager 2.

### 3.4 `Main_File_Custom_Mission.m`

**Details:** A script containing all definitions of dates, relevant mission information (sequence of bodies, real mission data for comparison, etc.), and PSO parameter definitions.

**Purpose:** Organize all function calls for a mission into one script for a new mission design from Earth to Saturn, using gravity assists of Venus and Jupiter respectively.

# References


[1] Curtis, H. D. (2014) *Orbital Mechanics for Engineering Students*, 3 ed., Butterworth-Heinemann.

[2] Labunsky, A. V., O. V. Papkov, and K. G. Sukhanov (1998) *Multiple Gravity Assist Interplanetary Trajectories*, Gordon and Breach Science Publishers.

[3] Minovitch, M. A. (2010) "The Invention that Opened the Solar System to Exploration," *Planetary and Space Science*, **58**(6), pp. 885–892.

[4] Minovitch, M. A. (1963) "The Determination and Potentialities of Advanced Free-Fall Interplanetary Trajectories." in *Proceedings of the First Graduate Academy of the University of California*, pp. 93–116.

[5] Casalino, L., G. Colasurdo, and D. Pastrone (1998) "Optimization of Delta-V Earth-gravity-assist Trajectories," *Journal of Guidance, Control, and Dynamics*, **21**(6), pp. 991–995.

[6] Diehl, R., D. Kaplan, and P. Penzo (1983) "Satellite Tour Design for the Galileo Mission," in *21st Aerospace Sciences Meeting*, p. 101, AIAA-83-0101.

[7] Peralta, F. and S. Flanagan (1995) "Cassini Interplanetary Trajectory Design," *Control Engineering Practice*, **3**(11), pp. 1603–1610.

[8] Vasile, M., J. M. R. Martin, L. Masi, E. Minisci, R. Epenoy, V. Martinot, and J. F. Baig (2015) "Incremental Planning of Multi-gravity Assist Trajectories," *Acta Astronautica*, **115**, pp. 407–421.

[9] Ceriotti, M. and M. Vasile (2010) "Automated Multigravity Assist Trajectory Planning with a Modified Ant Colony Algorithm," *Journal of Aerospace Computing, Information, and Communication*, **7**(9), pp. 261–293.

[10] Longuski, J. M. and S. N. Williams (1991) "Automated Design of Gravity-assist Trajectories to Mars and the Outer Planets," *Celestial Mechanics and Dynamical Astronomy*, **52**(3), pp. 207–220.

[11] Strange, N. J. and J. M. Longuski (2002) "Graphical Method for Gravity-assist Trajectory Design," *Journal of Spacecraft and Rockets*, **39**(1), pp. 9–16.

[12] Izzo, D., V. M. Becerra, D. R. Myatt, S. J. Nasuto, and J. M. Bishop (2007) "Search Space Pruning and Global Optimisation of Multiple Gravity Assist Spacecraft Trajectories," *Journal of Global Optimization*, **38**(2), pp. 283–296.

[13] Venditti, F. C. F., E. M. Rocco, A. F. B. de Almeida Prado, and A. Suhkanov (2010) "Gravity-assisted Maneuvers Applied in the Multi-objective Optimization of Interplanetary Trajectories," *Acta Astronautica*, **67**(9-10), pp. 1255–1271.

[14] Ovchinnikov, M. Y., S. P. Trofimov, and M. Shirobokov (2013) "Method of Virtual Trajectories for the Design of Gravity Assisted Missions," *Cosmic Research*, **51**(6), pp. 439–451.

[15] Chromey, F., B. Kaufman, and C. Newman (1966) "Gravity Assist Optimization Technique Applicable to a Variety of Space Missions," NASA X-507-66-373.

[16] Crain, T., R. H. Bishop, W. Fowler, and K. Rock (2000) "Interplanetary Flyby Mission Optimization Using a Hybrid Global-local Search Method," *Journal of Spacecraft and Rockets*, **37**(4), pp. 468–474.

[17] Wagner, S. and B. Wie (2015) "Hybrid Algorithm for Multiple Gravity-assist and Impulsive Delta-V Maneuvers," *Journal of Guidance, Control, and Dynamics*, **38**(11), pp. 2096–2107.

[18] Zuo, M., G. Dai, L. Peng, M. Wang, and J. Xiong (2016) "Multiple Gravity Assist Spacecraft Trajectories Design Based On BFS and EP/DE Algorithm," *International Journal of Aerospace Engineering*, **2016**.

[19] Eberhart, R. and J. Kennedy (1995) "A New Optimizer Using Particle Swarm Theory," in *Micro Machine and Human Science, 1995. MHS'95., Proceedings of the Sixth International Symposium on*, IEEE, pp. 39–43.

[20] Bessette, C. R. (2006) *Optimal Interplanetary Trajectories Via Evolutionary Algorithms*, Master's thesis, The Pennsylvania State University, State College, PA.

[21] Bessette, C. R. and D. B. Spencer (2007) "Performance Comparison of Stochastic Search Algorithms on the Interplanetary Gravity-assist Trajectory Problem," *Journal of Spacecraft and Rockets*, **44**(3), pp. 722–724.

[22] Pontani, M. and B. A. Conway (2010) "Particle Swarm Optimization Applied to Space Trajectories," *Journal of Guidance, Control, and Dynamics*, **33**(5), pp. 1429–1441.

[23] Rahimi, A., K. Dev Kumar, and H. Alighanbari (2012) "Particle Swarm Optimization Applied to Spacecraft Reentry Trajectory," *Journal of Guidance, Control, and Dynamics*, **36**(1), pp. 307–310.

[24] Zhao, J. and R. Zhou (2015) "Particle Swarm Optimization Applied to Hypersonic Reentry Trajectories," *Chinese Journal of Aeronautics*, **28**(3), pp. 822–831.

[25] Zotes, F. A. and M. S. Peñas (2012) "Particle Swarm Optimisation of Interplanetary Trajectories from Earth to Jupiter and Saturn," *Engineering Applications of Artificial Intelligence*, **25**(1), pp. 189–199.

[26] Melton, R. G. (2018) "Differential Evolution/Particle Swarm Optimizer for Constrained Slew Maneuvers," *Acta Astronautica*, **148**, pp. 246 – 259.

[27] Vallado, D. A. (2013) *Fundamentals of Astrodynamics and Applications*, 4 ed., Microcosm, Inc.

[28] Bate, R. R., D. D. Mueller, and J. E. White (1971) *Fundamentals of Astrodynamics*, Courier Corporation.

[29] Prussing, J. E. and B. A. Conway (2013) *Orbital Mechanics*, 2 ed., Oxford University Press, USA.

[30] Walter, U. (2008) *Astronautics*, John Wiley & Sons.

[31] Wiesel, W. E. (2010) *Spaceflight Dynamics*, 3 ed., Aphelion Press.

[32] Alan B. Chamberin, R. S. P. (2014), "JPL Planetary and Lunar Ephemerides," .
URL `https://ssd.jpl.nasa.gov/?planet_eph_export`

[33] Battin, R. H. and R. M. Vaughan (1984) "An Elegant Lambert Algorithm," *Journal of Guidance, Control, and Dynamics*, **7**(6), pp. 662–670.

[34] Lancaster, E. R. and R. H. Estes (1970) "A Universal Solution of Lambert's Problem," NASA TM X-65306.

[35] Shen, H. and P. Tsiotras (2003) "Using Battin's Method to Obtain Multiple-revolution Lambert's Solutions," *Advances in the Astronautical Sciences*, **116**, pp. 1067–1084.

[36] Izzo, D. (2015) "Revisiting Lambert's Problem," *Celestial Mechanics and Dynamical Astronomy*, **121**(1), pp. 1–15.

[37] Gooding, R. (1990) "A Procedure for the Solution of Lambert's Orbital Boundary-value Problem," *Celestial Mechanics and Dynamical Astronomy*, **48**(2), pp. 145–165.

[38] Knopf, W. (2018), "PDS: The Planetary Data System," .
URL `https://pds.nasa.gov/`

[39] McMahon, J. W. and D. J. Scheeres (2016) "Linearized Lambert's Problem Solution," *Journal of Guidance, Control, and Dynamics*, pp. 2205–2218.